Unique growth and morphology properties of Clade 5 *Clostridioides difficile* strains revealed by single-cell time-lapse microscopy

John W. Ribis[1,2], César Nieto[3], Nicholas V. DiBenedetto[1,2], Anchal Mehra,[4] Qiwen Dong[1], Irene Nagawa,[1] Imane El Meouche,[5] Bree B. Aldridge,[1,6] Mary J. Dunlop,[7] Rita Tamayo,[4] Abhyudai Singh,[3] Aimee Shen[1*]

Affiliations

[1]Department of Molecular Biology and Microbiology, Tufts University School of Medicine, Boston, Massachusetts, USA, [2] Graduate School of Biomedical Sciences, Tufts University School of Medicine, Boston, Massachusetts, USA. [3]Department of Electrical and Computer Engineering, University of Delaware, Newark, DE 19716, USA. [4]Department of Microbiology and Immunology, University of North Carolina at Chapel Hill School of Medicine, Chapel Hill, NC, USA, [5]INSERM, Université Paris Cité, Université Sorbonne Paris Nord, Inserm, IAME, F-75018, Paris, France, [6]Department of Biomedical Engineering, Tufts University School of Engineering, Medford, Massachusetts, USA, [7]Biomedical Engineering, Boston University, Boston, MA 02215.

[*]Address correspondence to
Aimee Shen, aimee.shen@tufts.edu
Phone number: (617)636-3792

Abstract

Clostridioides difficile is a major One Health threat as a gastrointestinal pathogen of both humans and agricultural animals. The *C. difficile* species consists of five main clades, with Clade 5 currently undergoing speciation from Clades 1-4. Notably, Clade 5 strains are highly prevalent in agricultural animals and can cause zoonotic infections, suggesting that Clade 5 strains have evolved phenotypes that distinguish them from Clade 1-4 strains. Here, we compare the growth properties of Clade 5 strains to Clade 1, 2, and 4 strains using anaerobic time-lapse microscopy coupled with automated image analysis. These analyses reveal that Clade 5 strains grow faster than Clade 1, 2, and 4 strains and are more likely to form long chains of cells. Comparative genomic analyses revealed that the orientation of the invertible *cmr* switch sequence likely drives the cell chaining phenotype of Clade 5 strains during growth in rich media. Interestingly, during murine infection, Clade 5 strains with a high frequency of the *cmr* switch in the ON orientation shifted to a largely *cmr* OFF state, suggesting that the *cmr* OFF state may be positively selected during infection. Taken together, our data suggest that Clade 5 strains have distinct growth properties that allow them to inhabit diverse ecological niches.

44 **Importance**

45 The Clade 5 strains of the *Clostridioides difficile* species are so phylogenetically divergent that
46 they almost meet the threshold of being a distinct species. Although these strains are
47 ubiquitously isolated from agricultural and environmental settings and an important source of
48 zoonotic and community-acquired infections, it is unclear whether they have distinct phenotypic
49 properties that allow them to efficiently colonize diverse hosts or persist in the environment. By
50 combining a novel anaerobic time-lapse microscopy method with automated image analysis, we
51 discovered that Clade 5 strains grow faster than strains from other *C. difficile* clades and that
52 they frequently form long chains. These chaining properties appear to be driven by the
53 environmentally responsive expression of a non-canonical signal transduction system, which we
54 also found is likely selected against during growth in mice. Collectively, our analyses reveal that
55 Clade 5 strains have distinct growth properties that may promote their persistence in the
56 environment.
57

58 **Introduction**

59

60 *Clostridioides difficile* is a leading cause of nosocomial infection in the United
61 States, with approximately 500,000 new infections and 14,000 deaths attributed to this
62 organism annually (1, 2). As an obligate anaerobe, *C. difficile* relies on its ability to form hardy,
63 metabolically dormant spores to survive outside the gut environment and transmit disease to
64 new hosts (3). When *C. difficile* spores are ingested by susceptible hosts (4, 5), they germinate
65 and outgrow into vegetative cells that subsequently colonize the colon. The vegetative cells
66 secrete toxins that damage gut epithelial tissue (6), which triggers a significant inflammatory
67 response that can cause disease pathologies ranging from mild diarrhea to pseudomembranous
68 colitis and even death (2, 4). *C. difficile* also causes recurrent infections (~20% of infections),
69 which can lead to more severe disease symptoms (2, 7, 8).

70 *C. difficile*'s success as a pathogen may be related to its tremendous genetic diversity (9-
71 11). Genomic analyses indicate that *C. difficile*'s core genome represents only ~10-20% of its
72 pan-genome (9, 10). The plasticity of its "open" pan-genome likely helps *C. difficile* colonize
73 the gastrointestinal tract of diverse animals, from mammals to invertebrates, and persist in
74 environmental reservoirs like sewage and compost (12). Multi-locus sequence typing (MLST)
75 analyses have revealed that the *C. difficile* species comprises five distinct phylogenetic clades
76 that can be further subdivided into different ribotypes (RTs) or sequence types (STs) (10, 13).

77 Between these five clades, there are notable differences in geographic and host
78 distributions. Clade 1 is the largest and most heterogeneous clade, containing over 200 STs that
79 have the broadest geographic distribution (14, 15). It includes both toxin-producing and non-
80 toxigenic strains, including the well-characterized, genetically tractable toxigenic strain 630 (9).
81 Clade 2 harbors epidemic-associated strains found within the ribotype 027 (RT027) lineage.
82 Strains from this ribotype have been associated with outbreaks in hospitals, particularly in
83 North America, due to their frequent resistance to fluoroquinolones (16-18). These epidemic
84 strains can also cause severe disease symptoms in part due to their production of three toxins:
85 TcdA, TcdB, and CDT (binary toxin) (6). Although RT027 strains have frequently been
86 associated with "hypervirulence," there is considerable phenotypic diversity within this lineage
87 with respect to virulence, toxin production levels, and sporulation (19-21).

88 Clade 3 strains are relatively uncommon and harbor a unique cell surface due to their
89 lack of CwpV production (22), but phenotypic analyses of biofilm formation and motility
90 suggest that they share similarities with Clade 2 strains like R20291 (23). Clade 4 contains
91 RT017 (ST37) strains that only encode a single toxin, TcdB (i.e., $TcdA^{-}CDT^{-}$), and are often
92 clindamycin- and fluoroquinolone-resistant. RT017 strains have been associated with outbreaks
93 in Europe and North America and are the most common strains found in Asia (24). Clade 5 is
94 the most genetically distant from the other 4 main *C. difficile* clades (94) and is thought to have
95 emerged before Clades 1-4 (25). While the average nucleotide identity (ANI) for Clades 1-4
96 ranges between 97.1 - 99.8%, Clade 5 strains exhibit ANI values around 96%, which is close to
97 the ANI value demarcation used by NCBI to define organisms of the same species (10, 26).
98 Thus, Clade 5 strains appear to be actively diverging from Clades 1-4 (10).
99 Clade 5 strains are an increasing problem in healthcare and agricultural settings because
100 they can cause severe disease in humans and are commonly found in livestock, particularly pigs
101 (12, 27). While other *C. difficile* strains have been known to infect both humans and animals,
102 only Clade 5 strains have been associated with zoonotic transmission from both animal-to-
103 human and human-to-animal (27, 28). The mechanisms underlying this bidirectional zoonotic
104 transmission are poorly understood, but the increased carriage of antimicrobial resistance genes
105 by Clade 5 strains may contribute to their ability to persist in agricultural and community
106 settings (27, 29). Thus, Clade 5 strains are of particular relevance from a One Health
107 perspective (12, 30), especially since they frequently cause community-acquired infections (29)
108 and are often detected in retail foods (31). These observations highlight the importance of
109 understanding the unique properties of this group of strains. Indeed, a recent genomic analysis
110 suggests that RT078/ST11 strains within Clade 5 frequently carry zinc acquisition and
111 homeostasis genes (11).
112 Despite numerous genomic analyses revealing the remarkable genetic diversity of *C.*
113 *difficile* strains, relatively few studies have investigated the phenotypic diversity between strains
114 from different clades. Clade-specific differences in colony morphology between Clade 5 strains
115 relative to Clade 1-4 strains have been described in a limited set of analyses (25, 32), suggesting
116 that differences in growth and/or cellular morphology may exist within clades. While
117 differences in bulk growth rates between *C. difficile* strains have been reported (33), most
118 phenotypic analyses have been conducted on a limited subset of strains within a given clade.

119 Furthermore, systematic comparisons of the growth properties of the different clades or
120 comparisons of cell morphology have not been performed to date.
121 Here, we compare the growth properties of multiple strains derived from the four
122 predominant main phylogenetic clades of *C. difficile* (Clade 1, 2, 4, and 5) using anaerobic
123 time-lapse microscopy. These analyses unexpectedly revealed striking differences in the growth
124 and cell morphology of the Clade 5 lineage relative to strains from Clades 1, 2, and 4.
125 Specifically, we found that Clade 5 strains grow faster and frequently form long chains, in
126 contrast with Clade 1, 2, and 4 strains. Genomic comparisons of the Clade 5 strains tested
127 strongly suggest that the presence of the *cmr* switch in the ON orientation drives their chaining
128 phenotype. While the orientation of this switch has previously been associated with cell
129 chaining (32), we found that Clade 5 strains with a strong *cmr* ON bias mostly reverted to a *cmr*
130 OFF phenotype during murine infection. Taken together, our data reveal that Clade 5 strains
131 have unique growth properties relative to Clade 1, 2, and 4 strains that may contribute to the
132 improved ability of Clade 5 strains to colonize and persist in a wider range of animal hosts.
133

134 **Results**

135

136 **Development of a simple method for time-lapse imaging under anaerobic conditions**

137

138 Time-lapse imaging of single cells has been widely used in bacteria due to the growing
139 appreciation that clonal bacterial populations can exhibit considerable phenotypic heterogeneity,
140 which can impact antibiotic resistance and virulence (32, 34-37). However, live single-cell
141 analyses in *C. difficile* have been complicated by its inability to grow in the presence of
142 atmospheric oxygen (38). While there have been limited reports of live cell time-lapse
143 microscopy of *C. difficile*, these analyses have required custom growth chambers to maintain
144 anaerobic conditions (39), which may limit the accessibility of these experimental systems to
145 most investigators.
146 To overcome these limitations, we established a simple system that relies solely upon
147 commercially available reagents and materials to grow *C. difficile* cells under anaerobic
148 conditions. This system uses gas-tight, adhesive Gene Frames™, which have been used
149 extensively in imaging applications for bacteria (40). Notably, the gas-impermeability of these

150 commercial seals allows anaerobic conditions to be maintained when agarose pads made with
151 growth media are prepared in the anaerobic chamber (**Figure 1**). Gene Frames also generate
152 thick agarose pads, which are critical for *C. difficile* to grow in a sealed system under ambient
153 conditions. Upon preparing agarose pads in the anaerobic chamber, *C. difficile* cultures are
154 inoculated onto the pads, and the pads are sealed a coverslip. At this point, the growth chamber is
155 removed from the chamber and imaged on a heated stage under ambient conditions for up to 6
156 hours. Although the growth chamber maintains its anaerobic status during this time, movies were
157 generally limited to 6 hours because *C. difficile* stopped growing exclusively as a monolayer.
158

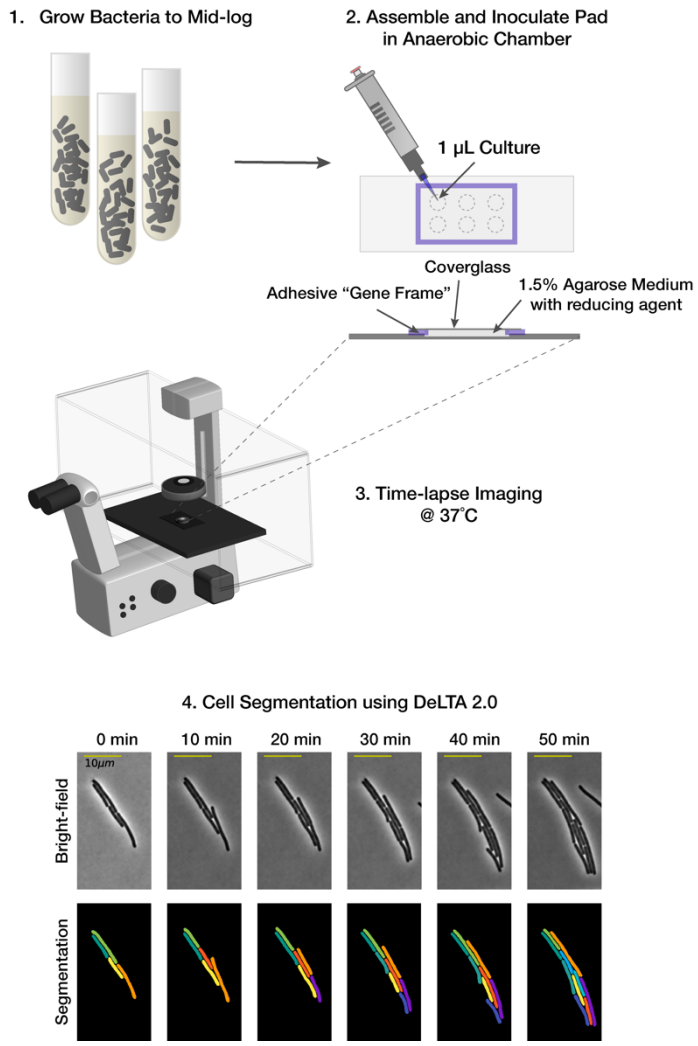

159
160

161 **Figure 1. Schematic of the anaerobic single-cell imaging set-up**. Exponentially growing *C. difficile*
162 cells in TY medium supplemented with cysteine (TYC) are spotted onto 1.5% agarose pads formed
163 within gas-tight adhesive Gene Frames inside the anaerobic chamber. Up to 6 strains can be spotted
164 onto a pad. The pad is sealed with a coverslip, and the imaging chamber is removed from the anaerobic

165 chamber and transferred to a heated (37˚C) microscope stage. Time-lapse microscopy is used to
166 visualize the growth of individual bacterial cells for 2-6 hrs. The output data is segmented and tracked
167 with the DeLTA Python package (191). An example filmstrip of strain 630 grown on TYC medium
168 over time is shown (Bottom).
169

170 **Time-lapse microscopy reveals clade-specific differences in elongation rate and cell length**

171

172 With the establishment of our time-lapse imaging setup, we compared the single-cell
173 growth properties of representative *C. difficile* strains from Clade 1 (630, ribotype (RT) 012),
174 Clade 2 (R20291, RT027), Clade 4 (M68, RT017), and Clade 5 (M120, RT078) (**Figure 2,**
175 **Table 1**). We did not have access to Clade 3 strains, so these were not included in this study.
176 The four "representative" strains were all isolated from patients with *C. difficile*-associated
177 disease and are frequently used as reference genomes for their clades and ribotype groups.
178 Notably, RT027 (ST1), RT017 (ST45), and RT078 (ST11) strains are from ribotypes/ multi-
179 locus sequencing types that are frequently isolated from patients with *C. difficile* infection
180 (CDI) (12, 16, 19, 24).
181 To quantify the growth properties of single cells visualized by time-lapse microscopy,
182 we used the Deep Learning for Time-lapse Analysis (DeLTA) software to rapidly and
183 accurately segment and track bacteria growing in two dimensions on agarose pads (41, 42).
184 This software uses deep convolutional neural networks to analyze time-lapse microscopy
185 images, allowing us to obtain information on the growth properties of individual cells growing
186 in microcolonies on agarose pads. The segmentation and tracking of *C. difficile* cells were
187 highly accurate (**Figure 1**), and minimal user input or post-image processing was needed to
188 obtain growth property measurements.
189 Robust growth was observed for all strains using our system. We quantified growth
190 using the elongation rate defined as doublings/hr. Notably, the Clade 5 strain M120 elongated
191 the fastest (2.1 doublings/hr), followed by Clade 2 strain R20291 (1.8 doublings/hr), and then
192 Clade 1 strain 630 and Clade 4 strain M68 (1.6-1.7 doublings/hr) (**Figure 2A**). The elongation
193 rate was defined as doublings/hr to indicate the number of times that a cell's size doubles in one
194 hour. Notably, the elongation rate (doublings/hr) should not be confused with doubling time, or
195 generation time, which represent the length of *time* that it takes before a bacterium divides.
196 Instead, the elongation rate reflects how fast the cell is increasing in length over time.
197

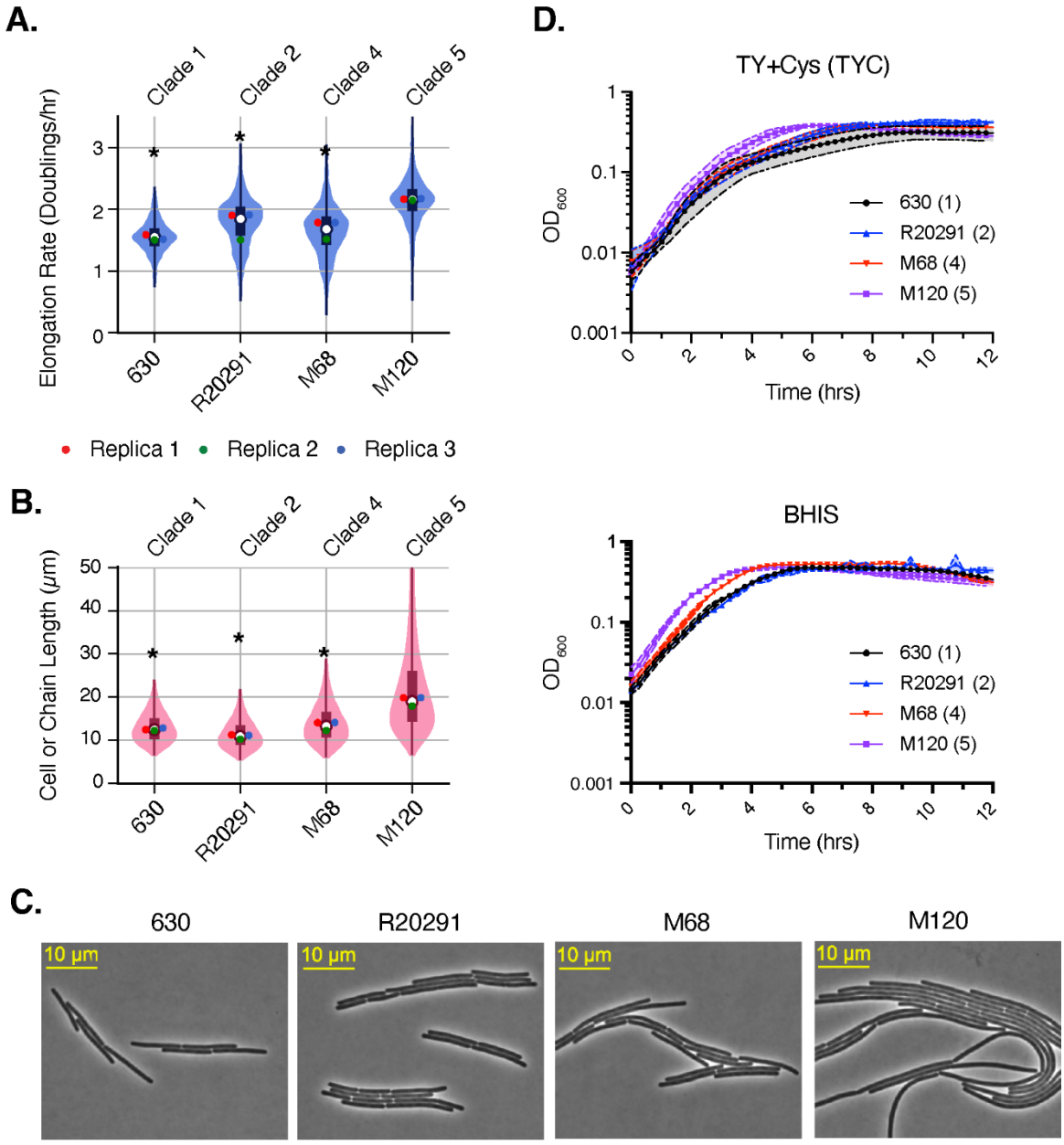

Figure 2. Clade 5 strain M120 elongates more quickly and exhibits cell chaining. (A) Violin plot of the elongation rates measured during time-lapse microscopy analyses of strains 630 (Clade 1), R20291 (Clade 2), M68 (Clade 4), M120 (Clade 5) grown on TY supplemented with cysteine (TYC) agar. Data are from three biological replicates, with the mean of each replicate shown as a point on the violin. (B) Violin plot of the cell or chain length measured during time-lapse microscopy for strains 630 (Clade 1), R20291 (Clade 2), M68 (Clade 4), M120 (Clade 5). Each replicate mean is shown as a point on the violin. Statistical significance for A and B was determined by comparing the mean of the three replicates of Clade 1, 2, and 4 strains relative to the Clade 5 M120 strain using a Kruskal-Wallis test * $p < 0.05$. (C) Phase-contrast image from time-lapse microscopy movies. Scale bar is 10 µm. D. Optical density-based analyses of bulk population growth of the indicated strains in TYC or BHIS medium. The number in brackets indicates the clade to which a given strain belongs.

212 Importantly, the differences in single-cell elongation rates measured for the four strains
213 using DeLTA were also observed in bulk population analyses of their growth using optical
214 density in TYC and BHIS media (**Figure 2D**). These analyses confirmed that the Clade 5 strain
215 M120 grows faster (using optical density as a proxy for bacterial growth) than the Clade 1, 2,
216 and 4 strains analyzed. In contrast, negligible differences in bulk growth rates were observed
217 between Clade 1, 2, and 4 strains (**Figure 2D**), consistent with the relatively subtle difference
218 observed in the single-cell elongation rates measured for the Clade 2 R20291 strain relative to
219 the Clades 1 and 4 strains (**Figure 2A**).
220 The Clade 5 strain M120 exhibited another distinct growth property from the strains
221 from Clades 1, 2, and 4. While strains from Clades 1, 2, and 4 produced cells of similar length
222 prior to cell division, with an average length of ~13 µm, cells of Clade 5 strain M120 were
223 significantly longer, appearing as chains with an average length of 22 µm; M120 chains of ~50
224 µm were also readily observed (**Figure 2B**), and chains appeared to bend readily (**Figure 2C**).
225 Notably, to fully visualize the chains made by M120, it was necessary to stitch together several
226 fields of view. This modification revealed that some M120 chains approached several hundred
227 microns and even up to ~1 mm in length (**Figure 3**). By incorporating the lipophilic fluorescent
228 dye FM4-64 into the agarose pads to visualize cell membranes (43), we determined that strain
229 M120 forms chains rather than filaments based on the presence of division septa throughout the
230 length of the cell (**Figure 3, inset**). Notably, the spacing between division septa was relatively
231 similar to the other *C. difficile* strains analyzed, suggesting that Clade 5 strain M120 undergoes
232 cell separation less efficiently than strains from the other clades tested.
233

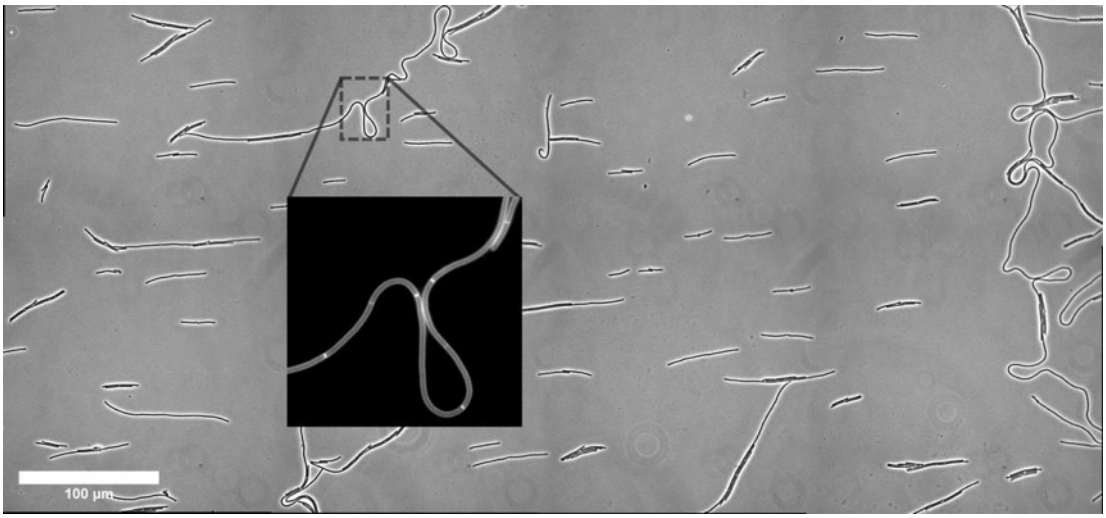

234

235
236 **Figure 3. *C. difficile* Clade 5 can form large heterogenous chains.** Large mosaic phase-contrast
237 image of the Clade 5 strain M120. Zoomed image shows chains revealed by staining with the
238 membrane dye FM4-64. Image was stitched from 8 individual fields of view at 63x magnification.
239 Scale bar is 100 µm.
240

241 **Clade 5 clinical isolates typically form long chains and grow more quickly than strains**
242 **from other clades**
243

244 Since prior work indicated that Clade 5 strains produce colony morphologies distinct from
245 Clade 1, 2, and 4 strains (25), we sought to determine whether the striking cell chaining
246 phenotype and faster growth rate observed in Clade 5 strain M120 were properties shared by
247 other Clade 5 strains. Thus, we compared the single-cell growth properties of five additional
248 Clade 5 clinical isolates obtained from three separate hospitals on TYC agarose (**Table 1**) using
249 time-lapse microscopy analyses (**Figure 2**). Clade 1 strain 630 was included as a control since it
250 does not form chains under these conditions.
251 These analyses revealed that all but one of the Clade 5 strains tested formed long chains, with
252 TAL29600 forming the longest chains (29 µm on average, **Figure 4A-C**). In contrast, strain
253 TAL29996 formed shorter chains that were comparable in length to those observed for strains
254 from Clades 1, 2, and 4 (12-13 µm, **Figures 2B, 4C**). Notably, DeLTA segmented most Clade 5
255 strains as single cells because it was unable to identify division septa (based on FM4-64
256 staining) within a given chain because cell separation had not yet been initiated. To overcome
257 this limitation and accurately quantify cell length within long chains, namely the distance
258 between division septa, we modified our image processing pipeline to use a thresholding
259 method to detect division septa. After generating masks in DeLTA to segment the chains, we
260 modified the mask so that only the interior of the contour was analyzed. We then applied an
261 adaptive thresholding method to identify division septa based on their elevated fluorescence
262 relative to the long axis of the cell; the thresholds were defined using a Gaussian-weighted
263 method (**Figure 4A**, red dots, **Figure 4B**). These analyses revealed that the average length of
264 cells made by Clade 5 strains that form long chains is only slightly longer than the average
265 length of cells made by strains that do not form chains. Specifically, the Clade 5 strains that
266 produced the longest chains (TAL29600 and TAL30550) had average cell lengths of 14 and 12
267 µm, respectively, that were 30-50% longer than strains that do not form chains like strains 630

(Clade 1, 8.5 µm) and TAL29996 (Clade 5, 9.4 µm) (**Table 2**). Notably, even though the Clade 5 strain TAL29996 did not form chains, it still elongated at rates similar to those of other Clade 5 strains (2.1 doublings/hr vs. 1.7 doublings/hr for Clade 1 strain 630**, Figure 4D**).

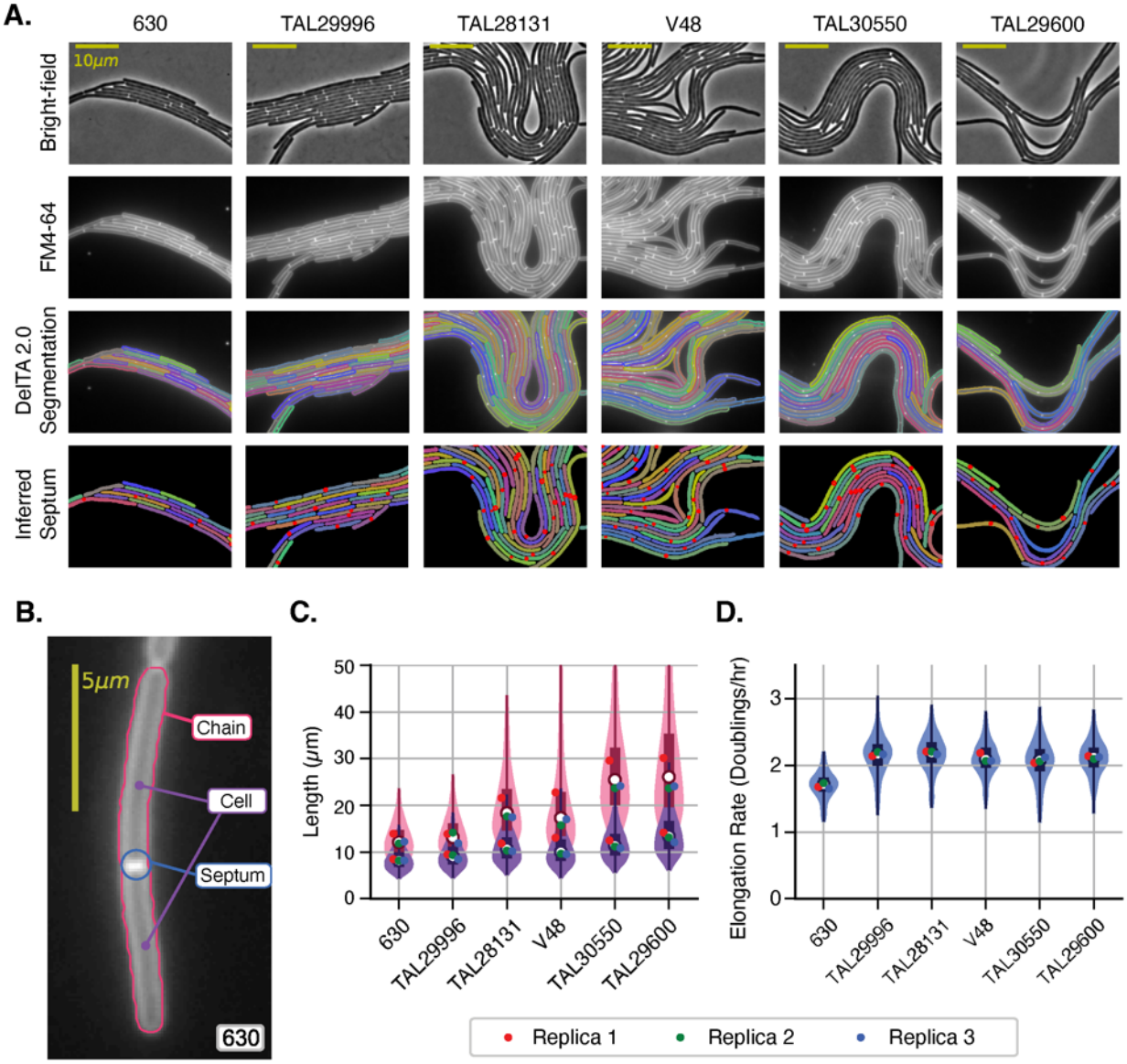

Figure 4. Faster growth is a common feature of Clade 5 strains, but the chaining phenotype is not fully penetrant in Clade 5 strains. (A) Phase-contrast microscopy images from time-lapse microscopy studies of Clade 5 strains; Clade 1 strain 630 is included for comparison. Fluorescence microscopy was used to visualize the FM4-64 stain incorporated into the agarose pads. Masks generated using DeLTA are shown, with the bottom panel showing division septa identified with our adaptive thresholding approach (red dots). (B) Example image showing the parameters identified using DeLTA combined with our adaptive threshold method for detecting division septa within a chain of cells. (C) Cell or chain length measured using automated DeLTA analyses (pink violin plot) or DeLTA combined with adaptive threshold analyses (purple violin plot). The former method is more likely to measure chain length, while the latter method accurately

283 measures cell length. (D) Violin plot of the elongation rates measured based on three biological replicates.
284 Each replicate mean is shown as a point on the violin; statistical significance was determined by comparing
285 the mean of the three replicates using a Kruskal-Wallis test, * $p < 0.05$.
286

287 Indeed, all the Clade 5 strains tested grew faster in bulk analyses in broth culture.
288 Specifically, in optical density-based analyses, the Clade 5 strains grew faster than Clade 1, 2,
289 and 4 strains irrespective of their ability to form chains or the growth medium used (**Figure S1**).
290 To assess whether these conclusions could be generalized to additional Clade 5 strains vs. Clade
291 1, 2, and 4 strains, we analyzed the growth of additional strains from all four clades in broth
292 culture. These analyses confirmed that Clade 1, 2, and 4 strains grow at similar rates, which are
293 slower than those measured for the nine Clade 5 strains analyzed in both TYC and BHIS media
294 (**Figure S1**). Taken together, these analyses strongly suggest that Clade 5 strains grow faster
295 than Clade 1, 2, and 4 strains and are more likely to form chains presumably because their cell
296 separation mechanisms are less efficient.
297

298 **Cell chaining in Clade 5 strains is not dependent on growth on a solid medium.**
299

300 *C. difficile* has previously been shown to promote cell elongation and chain formation
301 upon induction of the *cmrRST* locus (32), which encodes a non-canonical signal transduction
302 system. Expression of this locus is also responsive to c-di-GMP levels (44), which increases in
303 cells grown on solid surfaces such as in a biofilm or on an agar plate (44). To determine
304 whether the chaining phenotype observed in most Clade 5 strains is induced by growth on a
305 surface, we assessed whether cell chaining would be observed in cells grown in broth culture.
306 The Clade 5 strains, along with strains from other clades, were grown to log-phase in rich
307 media, and their ability to form chains was assessed by visualizing division septa with the
308 fluorescent D-amino acid label, HADA. Chains of cells were still observed in the Clade 5
309 strains during broth culture growth, although the chains formed in broth culture were not as
310 long as those observed during growth on the agarose pads (**Figure 5, S2**). Chains were also
311 observed in four additional Clade 5 strains analyzed during exponential-phase growth in broth
312 culture. Interestingly, two of the Clade 5 strains, V48 and WU66, failed to efficiently
313 incorporate the HADA label for unknown reasons, and the cells appeared lighter in phase-
314 contrast images despite undergoing the fixation process shortly after HADA addition (**Figure**

315 **S2**). Regardless, these results indicate that many Clade 5 strains undergo cell separation less
316 efficiently than strains from other clades irrespective of whether they are grown on a solid
317 surface or in broth culture.
318

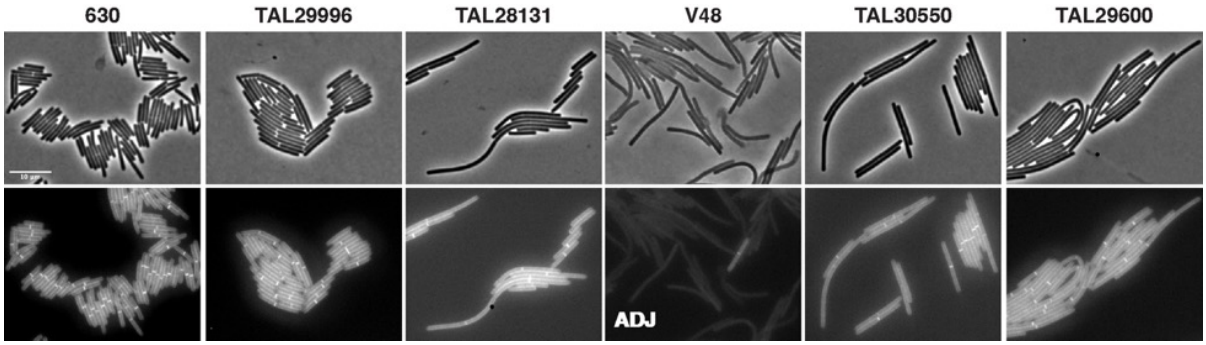

319
320
321 **Figure 5. Clade 5 strains form chains during logarithmic growth in broth culture**. Representative
322 micrographs showing phase-contrast (top) and peptidoglycan labeling with the fluorescent D-amino acid,
323 HADA, (bottom) following growth in rich broth (BHIS) to logarithmic phase. All strains shown with the
324 exception of 630 (Clade 1) are Clade 5 strains. Scale bar, 10 µm. Data are representative of multiple
325 independent experiments. **ADJ** indicates that the brightness of the image was enhanced to detect HADA
326 labeling in V48.
327
328 **Cell length does not correlate with the propensity to sporulate.**
329
330 We next wondered whether the propensity to form chains impacts the ability of Clade 5
331 strains to sporulate because analyses in *Bacillus subtilis* suggest that smaller cells, such as those
332 formed during stationary phase growth (45), may concentrate proteins involved in the
333 phosphorelay that induces sporulation (46, 47). Specifically, in *B. subtilis*, the decrease in cell
334 length helps the kinase KinA reach the threshold concentration needed to trigger sporulation
335 initiation. Although *C. difficile* lacks homologs of KinA and other components of the
336 phosphorelay system (48), it is possible that the longer cells generated by Clade 5 strains would
337 be less likely to induce sporulation due to dilution of a currently unknown sporulation regulator.
338 To test this hypothesis, we analyzed the propensity of Clade 5 strains to form spores when
339 plated on 70:30 sporulation medium using phase-contrast microscopy and heat resistance
340 assays. These analyses revealed that Clade 5 strains exhibit striking differences in sporulation
341 frequency, with some strains exhibiting close to 100% sporulation levels, and others exhibiting
342 levels closer to 20% (**Figure 6A, S3**). Strikingly, strain TAL29600 exhibited extremely low
343 levels of sporulation (0.003%). Despite this strain producing the longest chains, no correlation

344 between sporulation and cell length or chaining among the strains was observed (**Figure 6B,**
345 **S3**). For example, M120 forms long chains yet readily forms spores (~100% sporulation
346 frequency). The low sporulation levels of TAL29600 were rather surprising since this strain was
347 isolated from a clinical setting, so it likely forms spores more efficiently in conditions
348 encountered during infection. Interestingly, Clade 5 strains did not form long chains when
349 grown on 70:30 sporulation medium, and the spores produced by these isolates exhibited
350 similar lengths and proportions relative to the Clade 1 strain 630 (**Figure S4**). Thus, our data
351 suggest that Clade 5 strains alter their cell length and propensity to form chains depending on
352 the growth conditions encountered.

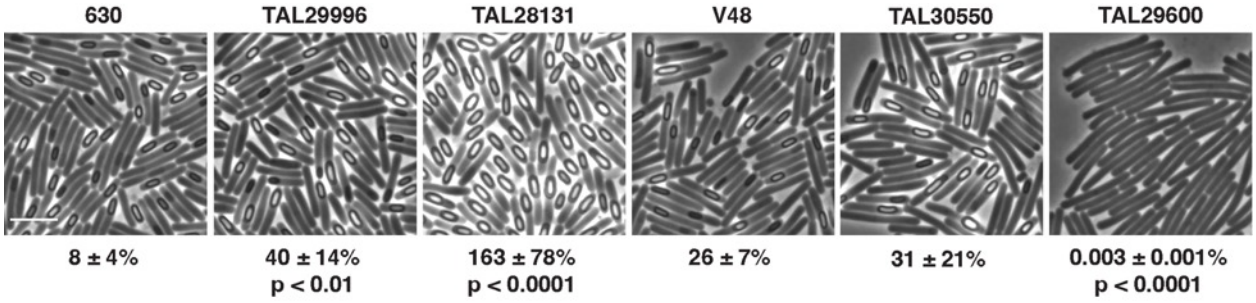

353
354
355 **Figure 6. Sporulation levels in Clade 5 isolates grown on 70:30 medium**. Phase-contrast microscopy
356 of the indicated strains ~24 hrs after sporulation induction. All strains shown with the exception of 630
357 (Clade 1) are Clade 5 strains. Heat resistance efficiencies, indicated below the respective images, are
358 based on 20-24 hr sporulating cultures and represent the mean and standard deviation for a given strain
359 relative to strain 630 based on a minimum of three biological replicates. Statistical significance relative
360 to strain 630 was determined using a one-way ANOVA and Tukey's test. The scale bar represents 5 µm.
361

362 **Genomic analyses of Clade 5 strains to identify putative loci controlling the chaining**
363 **phenotype**

364

365 Since our phenotypic analyses revealed that TAL29996 differs from the 8 other Clade 5
366 strains analyzed, we sought to gain insight into the molecular basis for this difference by
367 comparing their genomes. To this end, we sequenced 5 of the Clade 5 strains, including
368 TAL29996, and determined the average nucleotide identity (ANI) for orthologous genes. These
369 analyses revealed that the ANI between the strains ranging from 99.83-99.99% (**Table S1**). Since
370 the pan-genome between the 5 strains is 12%, they are quite closely related. A comparison of
371 their pan-genomes revealed that, relative to the other four strains, TAL29996 is missing one
372 duplication of *blaR1*, which encodes an integral membrane protein that senses beta-lactams, and
373 a gene region predicted to be involved in nicotinate metabolism. We also compared the genomes

374 using breseq (49) to identify SNPs that might distinguish TAL29996 from the other strains. We
375 used strain M120 as the reference genome, since this strain has been the Clade 5 strain
376 traditionally characterized (33, 50). Around 10 SNPs were unique to TAL29996, but none were
377 clearly implicated in regulating cell separation or peptidoglycan synthesis (**Table S2**).
378 Since none of the SNPs or absent genes led to hypotheses for why TAL29996 undergoes
379 cell separation more efficiently than the other Clade 5 strains, we took a candidate approach and
380 analyzed the orientation of the *cmr* switch, also known as the Cdi6 DNA invertible element (32,
381 51). The orientation of the *cmr* switch affects the expression of the adjacent *cmrRST* operon,
382 resulting in phase-variable production of the non-canonical CmrRST signal transduction system.
383 This system promotes cell chaining when produced. In addition, the orientation of the *cmr* switch
384 determines whether *C. difficile* produces rough or smooth colony morphologies (32, 44, 51).
385 Specifically, cells from rough colonies are highly biased to the ON orientation of the *cmr* switch
386 and exhibit a chaining phenotype, whereas cells from smooth colonies are highly biased to the
387 OFF orientation and do not form chains (32). Consistent with the breseq analyses, manual
388 inspection of the *cmrRST* upstream region revealed that this region is identical between all the
389 Clade 5 strains analyzed (100% identity), including strain TAL29996.
390 However, when we specifically assessed the orientation of the *cmr* switch during growth
391 in broth culture using qPCR, we found that Clade 5 strains form chains with a *cmr*-ON frequency
392 of between 70-96% on average (**Figure 7A**), whereas the *cmr*-ON frequency of the non-chaining
393 Clade 5 strain TAL29996 was greatly reduced (~20%, **Figure 7**). Furthermore, when we
394 extended these analyses to the four additional Clade 5 strains characterized that also produce
395 chains, we found that they exhibit a *cmr*-ON frequency of between 80-93%. Collectively, these
396 results suggest that a *cmr*-ON switch orientation correlates with the chaining phenotype observed
397 in the majority of Clade 5 strains even during growth in broth culture.
398
399 **Surface motility in Clade 5 strains relative to strains of other clades**
400
401 Since the *cmr*-ON state has also been correlated with increased surface motility, we analyzed the
402 surface motility of our Clade 5 strains. After a 5-day incubation, *cmr*-ON strains spread further
403 on agar plates than the TAL29996 *cmr*-OFF strain (**Figure 7B**). Consistent with prior reports
404 (32), Clade 5 strains whose *cmr* switch is predominantly in the ON orientation exhibited greater

405 and more uniform surface motility (**Figure 7**). In contrast, the surface motility of TAL29996 was
406 considerably reduced and more asymmetric, with fractal-like extensions extending from a couple
407 of sites. The surface motility of TAL29996 resembles the phenotype previously reported for
408 Clade 2 strain R20291, whose *cmr* switch is also predominantly in the OFF position in liquid
409 cultures (32).

410 However, growth of R20291 on agar medium selects for bacteria with the *cmr* switch in
411 the ON orientation, which leads to asymmetric surface motility on plates (32). These
412 observations suggest that, even though TAL29996 is biased to the *cmr*-OFF orientation during
413 broth culture growth, a subset of TAL29996 cells switch to the *cmr*-ON orientation during
414 growth on BHIS agar, leading to the asymmetric spreading phenotype.

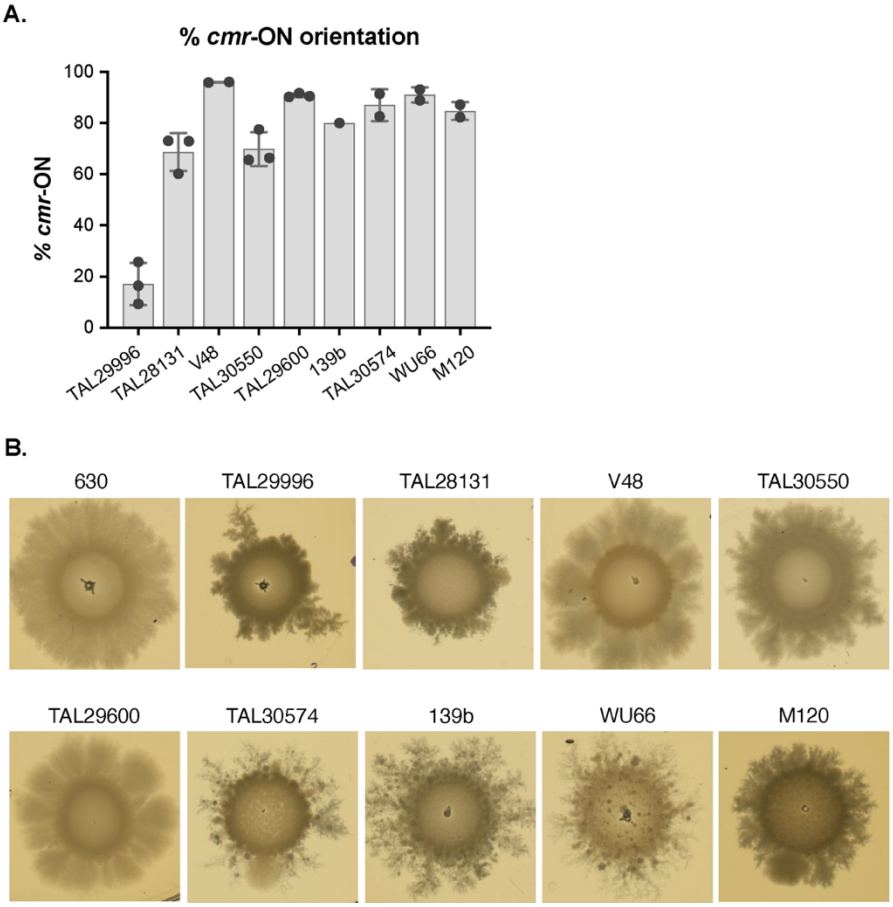

415
416

417 **Figure 7. Orientation of the *cmr* switch correlates with chaining phenotype and surface motility in**
418 **Clade 5 strains.** (A) Orientation-specific qPCR for detecting the orientation of the *cmr* switch in the
419 indicated strains. The mean and standard deviation based on one to three biological replicates are shown.
420 (B) Representative images of surface motility 5 days after exponentially growing liquid cultures were
421 spotted onto BHIS agar plates. All strains shown with the exception of 630 (Clade 1) are Clade 5 strains.
422

423 We next analyzed the propensity of Clade 1, 2, and 4 strains to exhibit surface motility.
424 These analyses revealed that asymmetric motility was more frequently observed in Clade 2
425 strains. Clade 1 strains exhibited a range of surface motility, from high surface motility with
426 strain 630 to lower surface motility with strain WU38 (**Figure S5**). While analyzing a larger
427 number of Clade 1, 2, and 4 strains would reveal whether there are clade-specific differences in
428 surface motility, the data suggest that *cmr* switching in Clade 2 strains is more variable between
429 strains during growth on agar medium, with strain Wup14 exhibiting the least surface motility of
430 the Clade 2 strains tested. Collectively, the data imply that the ON orientation of the *cmr* switch
431 during broth culture growth contributes to the chaining phenotype observed in most Clade 5
432 strains.
433
434 **Colonization and virulence properties of Clade 5 strains**
435
436 The *cmrRST* system impacts the virulence of the Clade 2 strain, R20291, in a hamster
437 model of infection, with loss of *cmrR* reducing R20291's ability to cause disease and the *cmr*-
438 OFF orientation correlating with less severe disease in hamsters (32). Since chaining in *Bacillus*
439 *anthracis* strains promotes virulence (52), while chaining in *Enterococcus faecalis* promotes
440 colonization (53), we compared the ability of Clade 5 strains to colonize mice and cause disease.
441 Specifically, we analyzed the ability of several Clade 5 strains and the Clade 1 strain 630 to
442 colonize and cause disease in antibiotic-treated mice. We also analyzed the orientation of the *cmr*
443 switch over the course of the 14-day infection for strains TAL29600 and TAL29996, which
444 exhibited the highest and lowest *cmr*-ON orientations, respectively, during growth in rich media
445 (**Figure 7A**).
446 All Clade 5 strains tested colonized to relatively similar levels for throughout the 14 days
447 of the infection. Strain 630 also colonized mice to similar levels in the first two days of infection
448 and then maintained colonization, albeit at 1-2 logs lower than the Clade 5 strains (**Figure 8A**).
449 Interestingly, only the Clade 5 strain TAL29600 caused significant weight loss relative to the
450 other strains on Days 2 through 4, while the Clade 1 strain 630 caused some weight loss on Day
451 3 (**Figure 8B**). This latter phenotype is consistent with prior reports of strain 630 causing only
452 mild disease symptoms in the cefoperazone model of murine infection (54, 55). Analyses of the
453 *cmr* orientation revealed that the *cmr*-OFF orientation appeared to be selected for over the course

454 of the infection. While the TAL29600 spore inoculum started off with ~30% *cmr*-ON frequency,
455 the frequency of TAL29600 cells detected in the *cmr*-ON orientation decreased rapidly to < 5%
456 *cmr*-ON by 24 hrs post-inoculation (**Figure 8C**). As the infection progressed, two of the 8 mice
457 tested exhibited an increase in TAL29600 cells with the *cmr*-ON orientation (6-30% *cmr*-ON)
458 (**Figure S6**). Conversely, the TAL29996 strain retained the ~1% *cmr*-ON frequency of the
459 inoculum for the greater part of the 14-day infection (**Figure 8C**). Taken together, these analyses
460 reveal that Clade 5 RT078 strains efficiently colonize mice but vary in their ability to cause
461 disease. Furthermore, the ability of the Clade 5 strains to colonize or cause disease did not
462 correlate with their ability to chain in rich media.
463

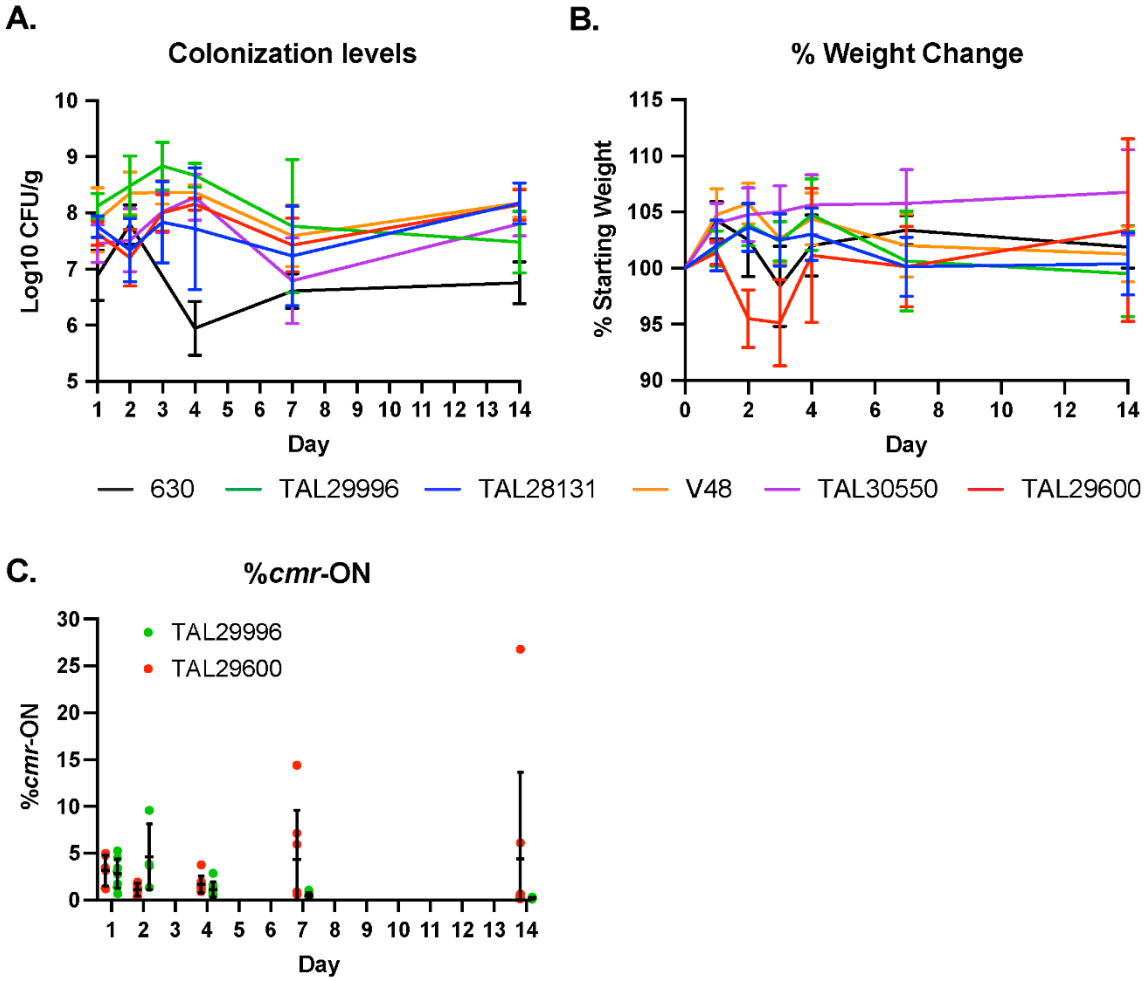

464

465 **Figure 8. Infection and colonization dynamics of Clade 5 strains in mice. (**A) Fecal colony-forming
466 units measured by selective plating and (B) Percentage of weight loss to baseline of infected mice on
467 Days 1-4, 7, and 14. The mean and standard deviation are shown based on the results of two experiments
468 consisting of four mice each (n = 8). (C) Percentage of *cmr* ON switch orientation measured in fecal
469 pellets on the indicated days by qPCR. For the strain TAL29996 inoculum, 1% of the spores had the *cmr*-

470 ON switch orientation, while the TAL29600 inoculum consisted of 32% *cmr*-ON spores. The mean and
471 standard deviation based on analyses of eight mice are shown, although fecal pellets could not be
472 collected from some of the mice on Day 2.
473

474 **Discussion**

475

476 While Clade 5 strains are genetically distinct from Clade 1-4 strains (10, 25) and more
477 prevalent in animals (12, 28, 29), the phenotypic impact of their genetic divergence has been
478 poorly characterized. By phenotypically characterizing *C. difficile* strains from multiple clades
479 using time-lapse microscopy, we discovered that Clade 5 strains have distinct growth properties
480 from the Clade 1, 2, and 4 strains tested. Specifically, Clade 5 strains elongate more quickly
481 (**Figures 2, 4, S1**) and form long chains more readily than strains from Clades 1, 2, and 4,
482 irrespective of media type or growth on a surface (**Figures 2, 4, S2**). In contrast, long chains
483 were not observed in any of the Clade 1, 2, and 4 strains, regardless of whether the cells were
484 grown on agarose pads or in broth culture. Thus, Clade 5 strains undergo cell separation far less
485 efficiently than strains from other clades during growth in rich media. While our analyses of
486 Clade 5 strains were largely limited to the RT078 ribotype, we note that a prior report described
487 an RT126 strain isolated from a patient experiencing multiple recurrences that also formed long
488 chains (56). Since the RT126 ribotype is closely related to the RT078 ribotype (12), the
489 chaining phenotype will likely be observed in other Clade 5 ribotypes.
490 Our data strongly suggest that the chaining phenotype of Clade 5 strains relates to their
491 propensity to have the *cmr* switch (32, 44) in the ON orientation during growth in rich media
492 (**Figure 7**) because the non-chaining TAL29996 strain exhibits a *cmr*-ON orientation frequency
493 of 20%, whereas the 8 other Clade 5 strains tested exhibit *cmr*-ON orientation frequencies of
494 ~70-95% (**Figure 7**). This conclusion is further supported by our finding that Clade 5 strains
495 form longer chains more frequently during growth on agarose pads compared to broth culture
496 (**Figures 4, 5**), which is similar to the finding that the *cmrRST* operon is induced by elevated c-
497 di-GMP levels encountered during growth on agar plates in the Clade 2 strain R20291 (44). In
498 addition, Clade 5 strains also exhibited high levels of surface motility, which is a *cmrRST*-
499 induced phenotype in strain R20291 (32). Interestingly, *cmrRST* expression is negatively
500 correlated with flagellar motility in strain R20291, and growth conditions favoring flagellar
501 motility select against *cmr*-ON bacteria in this strain (32). Since Clade 5 strains lack flagellar

502 motility (12), it is tempting to hypothesize that they are "primed" to exhibit surface motility.
503 Analyzing the regulation of c-di-GMP in different growth conditions in Clade 5 strains,
504 particularly for TAL29996 relative to the other strains, will likely provide insight into the
505 mechanisms that drive *cmrRST* expression, chaining, and surface motility in Clade 5 strains.
506 Such analyses would be greatly facilitated by methods for genetically manipulating Clade 5
507 strains.

508 While the propensity of Clade 5 strains to form chains and carry the *cmr* switch in the
509 ON orientation might be expected to promote colonization or disease in mice based on studies
510 of other Gram-positive pathogens (52, 53), we observed that the frequency of *cmr*-ON cells
511 decreases during the first 4 days of infection for strain TAL 29600 (**Figure 8**). This suggests
512 that there may be a selection against *cmr*-ON cells during the initial stages of murine
513 colonization. Indeed, a similar selection for the *cmr*-OFF orientation was observed during
514 infection of hamsters with R20291 (32). However, since the frequency of *cmr*-ON TAL29600
515 cells increased in some mice at later stages of colonization (**Figure 8**), our data imply that the
516 invertibility of the *cmrRST* switch region likely promotes *C. difficile*'s ability to adapt to
517 different growth conditions. While it is possible that the operon is expressed during infection
518 even if the orientation of the *cmr* switch is in the "OFF" position due to the induction of the
519 *cmrRST* operon by c-di-GMP (44), assessing whether Clade 5 strains form long chains during
520 murine infection, for example, using fluorescence *in situ* hybridization (57, 58) or using
521 transcriptional reporters to visualize the expression of the *cmrRST* operon at the single-cell level
522 during infection would allow these questions to be addressed.

523 It was also somewhat surprising that the five Clade 5 strains analyzed during murine
524 infection caused minimal to no disease (**Figure 8**) given that all of these strains were isolated
525 from human patients experiencing CDI-related disease symptoms (**Table 1**). To our knowledge,
526 very few Clade 5 strains have been analyzed during murine infection, with one study observing
527 minor disease symptoms in mice for two Clade 5 strains three days post-infection, despite one
528 of the strains causing severe disease in humans (20). Interestingly, RT078 Clade 5 strains
529 frequently cause asymptomatic infections in agricultural animals (31, 59) and mice may be
530 important vectors of transmission in these settings (60, 61). Thus, it is intriguing that our
531 preliminary analyses suggest that Clade 5 strains persist at high levels in the murine gut over
532 time compared to the Clade 1 strain 630 (**Figure 8**, $p < 0.005$, except TAL29996). Identifying

533 factors that allow Clade 5 strains to grow more quickly would provide critical insight into
534 whether this faster growth rate contributes to the persistence of these strains in mice.
535 Another unexpected finding was that the chain length of Clade 5 strains does not
536 correlate with their propensity to sporulate (**Figure 6**) because the strains tested varied wildly in
537 their sporulation frequencies. Overall, Clade 5 strains sporulated at high levels (>30%), with the
538 exception of strain TAL29600, which sporulates ~5,000-fold less efficiently than the other
539 Clade 5 strains, **Figure 6**). While little is known about the mechanisms regulating sporulation
540 initiation outside of strains 630 and R20291, future analyses of strain TAL29600, which
541 sporulates poorly under laboratory conditions (**Figure 6**) but not during murine infection
542 (**Figure 8**), could provide insight into the molecular determinants of sporulation initiation in
543 Clade 5 strains. For example, differences in gene presence or polymorphisms in several c-di-
544 GMP-related genes were observed in TAL29600 relative to the other Clade 5 strains (**Table**
545 **S2**), and c-di-GMP has also been implicated in regulating sporulation initiation events through
546 an unknown mechanism (62, 63).
547 Finally, a key finding of our time-lapse microscopy analyses is that *C. difficile* strains
548 generally undergo cell separation inefficiently after cell division, leading to the formation of
549 chains of two cells (Clades 1, 2, and 4) or long chains (most Clade 5 strains). While there was a
550 significant delay between cell division and cell separation in the latter case, the Clade 1 strain
551 630 and Clade 5 strain TAL29996, formed chains of two cells that were typically detected by
552 DeLTA as a single cell because cell separation had not yet initiated (**Figure 4**, red dot). Thus,
553 cell division and cell separation in *C. difficile* are not as tightly correlated as they are in many
554 bacteria.
555 The lack of coordination likely relates to the absence of FtsEX homologs in *C. difficile*,
556 which couple septal PG synthesis with PG hydrolases that mediate cell separation (64-67).
557 Indeed, recent work has identified novel factors that control cell chaining in *C. difficile*. The
558 CwlA peptidoglycan hydrolase is required for cell separation (68), and its activity is controlled
559 by the Ser/Thr kinase PrkC: phosphorylation inhibits cell separation by preventing CwlA export
560 (68). Since the septum-localizing MldA or MldB proteins also promote chaining in *C. difficile*
561 through unknown mechanisms (69), future work could address whether the inefficient cell
562 separation phenotype of Clade 5 strains is due to decreased CwlA export or MldA/MldB levels.

563 Importantly, our insights into the basic physiology of *C. difficile* were enabled by our
564 development of a facile method for conducting time-lapse microscopy under anaerobic
565 conditions. We anticipate that the methods used in this manuscript can be applied by many
566 anaerobic microbiologists to study the growth properties of their organisms(s) of interest, under
567 different conditions and mutant backgrounds. This is because the growth chamber set-up
568 involves only commercially available GeneFrames and open-source software for rapidly
569 conducting automated image analyses of time-lapse microscopy data (41, 42). Our anaerobic
570 set-up could be further coupled with recently developed, fluorogen-activated anaerobic imaging
571 tags (70) to facilitate single-cell analyses of gene-specific transcription during anaerobic growth
572 and dynamic protein localization studies (71). Thus, there are many potential applications for
573 the simple methods described here for studying the growth of anaerobes over time at the single-
574 cell level.
575
576 **Materials and Methods**
577
578 *Bacterial strains and growth conditions*
579 All *C. difficile* strains were grown on brain heart infusion (BHIS) medium supplemented
580 with 0.5% w/v yeast extract and 0.1% w/v L-cysteine with taurocholate (TCA; 0.1% w/v; 1.9
581 mM). Strains were sub-cultured into tryptone yeast extract (TY) broth supplemented with 0.1%
582 w/v L-cysteine (TYC medium) prior to inoculation onto the time-lapse microscopy agarose
583 pads. All strains were grown at 37°C under anaerobic conditions using a gas mixture of 85%
584 hydrogen, 5% CO2, and 10% H2. For time-lapse experiments, 1.5% agarose pads supplemented
585 with TYC medium were used as described above. Sporulation analyses were carried out on
586 70:30 medium (70% BHIS and 30% SMC) for 24h as described previously (72).
587
588 *Anaerobic time-lapse imaging of C. difficile growth*
589 All imaging was carried out on a Leica DMi8 inverted microscope with a HC plan
590 apochromat 63x 1.4 NA oil immersion phase contrast objective. Fluorescent membrane staining
591 experiments were done with a Lumencor Spectra X light source, coupled with an XLED-QP
592 quadruple-band dichroic beam-splitter (Leica) (transmission: 415, 470, 570, and 660 nm) along
593 with an external emission filter wheel (Leica). FM4-64 was excited using a 470nm LED
594 through a 470/20nm excitation filter and emitted light was filtered through a 590/50nm
595 emission filter and captured with a Leica DFC9000GTC sCMOS camera. All experiments were
596 carried out at 37°C using a microscope incubation system (Pecon), Leica Adaptive Focus
597 Control hardware autofocus, and a high precision stage (Pecon) were used for all imaging
598 experiments.
599 For time-lapse imaging of *C. difficile* growth, all bacterial strains were grown in 2 mL
600 liquid TY medium to a turbid OD600 > 2-3; after 2 hours of growth, bacteria were diluted 1:100
601 for Clade 5 strains and all other strains were diluted 1:50 in fresh media and grown to mid-log
602 phase (OD600 0.4-0.7).

603 An imaging chamber with a gas-tight seal was constructed using a 125 µL Gene
604 Frame (Thermo Fisher) adhered to a glass slide generating a well for growth medium. The slide
605 was then transferred to the anaerobic chamber. In the anaerobic chamber, the gene frame was
606 filled with 500µl 1.5% Top vision low melting point agarose and tryptone yeast extract media
607 containing 0.1% w/v L-cysteine to scavenge oxygen and maintain anaerobic conditions. While
608 the agarose was molten, a second clean slide was placed over the top and the agar pad was
609 placed on a frozen small freezer block (for holding PCR strip tubes) for 10-30 minutes until the
610 agarose-media mixture was solid. For experiments using FM4-64, agarose pads were made the
611 same way, with the addition of FM4-64 to a final concentration of 1 µg/mL directly to the
612 agarose/media solution prior to making the agar pad.
613 The agar pad was dried for 5-10 minutes until visible liquid on the surface of the pad
614 was evaporated. 1 µL of mid-log cells were spotted on the pad, dried, and a #1.5 coverslip
615 (VWR) was adhered to the Gene Frame. The cells were imaged at 37°C until they reached
616 confluency in the field of view. This was anywhere from 2.5 hours for Clade 5 strains to 6 hours
617 for Clades 1-4 for all experiments with images taken at 5-minute intervals.
618
619 *Image analysis, computing hardware, and statistical analysis.*
620 All movie frames were trimmed to the point when cells were not overlapping and out of
621 focus regions were cropped. The resulting images were analyzed using the Python library
622 DeLTA 2.0 (41, 42). All image and data analyses were done on a PC running Windows 10
623 equipped with an AMD Ryzen 5900HX 8-core CPU, 32GB DDR4 RAM, 2 1TB NVME SSDs,
624 and an NVIDIA RTX3080 GPU with 16GB VRAM. Analysis of the output data and data
625 visualizations were done in Python using Matplotlib/Seaborn, Pandas, Numpy, Scipy, and the
626 Statannotations library.
627
628 *Septum detection during live-cell microscopy*
629 The image processing starts with the masks generated using DeLTA 2.0. First, we performed
630 erosion on the mask with a disk of radius of 1 pixel to avoid effects of membrane fluorescence.
631 The photo was cropped following the eroded mask contour. Hence, only the interior of the
632 contour was considered. Pixel values were rescaled such that the minimum pixel value of inner
633 pixels was mapped to 0 and the maximum was mapped to 255. We set a threshold intensity as
634 the pixel value of the 95% quantile of pixel intensities. The image was slightly blurred by
635 convolution with a Gaussian filter with standard deviation of 2 pixels. The septum corresponds
636 to the contours found after performing an adaptive thresholding based on thresholds defined
637 using a Gaussian-weighted method. This thresholding was performed using the open cv2 library
638 in Python. The resultant contours were manually verified from videos generated using the
639 tracking from the outputs from DeLTA. The manual validation mainly involved filling in the
640 time points where the algorithm missed a ring that was visible in the video. We did not assume
641 the existence of a ring if the algorithm did not detect it in a previous frame.
642
643 *Cell length estimation*
644 We measured the cell projected area from the DeLTA contours of the images as the pixel amount
645 of the contours. However, estimating cell length was challenging because some cells were very
646 long and bent. To overcome this problem, we selected 30 images of three different cells (from
647 strains 630, TAL3050 and TAL28131) that were straight and had different lengths. For these
648 cells, we calculated the cell length as the longest side of the minimum bounding rectangle of the
649 contour. From these lengths of straight cells, we also estimated the best cell width as the average

650 of the projected area divided by the length. Considering the extreme cell length, the effects of the
651 rounded tips were negligible and the rectangle shape adequately approximated length. We
652 verified that this mean value showed low variability for the three strains. Then, we used this
653 width value to estimate the length of all the cells, including the bent ones, by dividing their
654 projected area by the width. This way, we obtained a consistent measure of cell length that was
655 independent of bending.
656
657 *Elongation rate estimation*
658 We tracked cell size over time and identified the division points as the ones where the cell size
659 (projected area) dropped by more than 30% compared to the current cell size value. We fitted an
660 exponential function (with base e) of time to the data points between two divisions and estimated
661 the elongation rate from the exponent of the best fit. We expressed the elongation rate in
662 doublings/hr, which means how many times the cell size doubles in one hour. For example, an
663 elongation rate of 2 doubling/hr means that the cell size doubles two times in 1 hr, which
664 corresponds to an exponent of 2ln(2) 1/hr. For the statistics, we only included the elongation
665 rates that had a high quality of fit, with an R2 coefficient greater than 0.9.
666
667 *Bulk growth measurements*
668 Starter cultures were grown until early stationary phase in BHIS (or TYC medium as indicated)
669 then diluted 1:50 into BHIS (or TYC medium). When the cultures reached an OD_{600} of 0.5, they
670 were diluted 1:25 into 200 µL of either BHIS or TYC in a flat 96 well polystyrene plate
671 (CellTreat). The OD_{600} was analyzed every 15 min for 24 hrs in a BioTek Epoch plate reader
672 with shaking. Bulk growth measurements are based on a minimum of three independent
673 replicates across a minimum of 2 experiments.
674
675 *Cell wall labeling*
676 HADA (Tocris Bioscience) was added to exponentially growing cell culture to a final
677 concentration of 50-100 µM and incubated for ~2 mins before cell fixation. Cells were fixed as
678 previously described (73). Briefly, 400 µL of cell suspension was added to 100 µL of a 5X
679 fixation solution containing paraformaldehyde and $NaPO_4$ buffer. Samples were mixed and
680 incubated in the dark for 30 min at room temperature, followed by 30 min on ice. Fixed cells
681 were washed three times in phosphate-buffered saline (PBS) and resuspended in ~50 µL of PBS.
682 Cells were imaged within 72 hours after fixation.
683
684 *Sporulation assays*.
685 Starter cultures were grown until early stationary phase in BHIS then diluted 1:50 into BHIS.
686 When the cultures reached an OD_{600} between 0.35 and 0.75, 120 µL of the culture was spread
687 onto 70:30 (70% SMC media and 30% BHIS media) agar plates (40 ml media per plate) and then
688 incubated for 20-24 hrs before the sporulating cells were scraped from the plate into phosphate-
689 buffered saline (PBS). Sporulation levels were visualized by phase-contrast microscopy as
690 previously described (74).
691
692 *Heat resistance assay.*
693 Heat-resistant spore formation was measured 20-24 hrs after sporulation was induced on 70:30
694 agar plates as previously described (72). The percent sporulation of given culture represents the
695 ratio of heat-resistant colony-forming units (CFUs) to total CFUs. Percent sporulation was
696 determined from a minimum of 3 biological replicates.

697
698 *Spore purification.*
699 Spores were purified as previously described (75) by scraping up sporulating cells incubated on
700 70:30 medium for 3 days into ice-cold H_2O. The cells were washed several times in ice-water
701 over the course of a day and incubated on ice overnight. The following morning, the sample was
702 pelleted, and cells were suspended in 1 X DNAse buffer (New England Biolabs) and then treated
703 with DNAse (New England Biolabs) for 30 min at 37˚C. The samples were washed one more
704 time before being resuspended in 20% Histodenz and then layered onto a 50% Histodenz layer.
705 The resulting mixture was pelleted, and the supernatant was aspirated off using a vacuum
706 aspirator. The pelleted spores were washed in ice-cold water 2-3 times and the optical density of
707 the purified spores was measured.
708
709 *Genomic DNA preparation*.
710 Starter cultures were grown until early stationary phase in BHIS then back-diluted 1:50 into
711 BHIS and grown until an OD_{600} of around 0.7-0.8 was reached. 10 mL of the culture was
712 pelleted and then frozen at -80˚C. After thawing the sample, it was resuspended in a 25%
713 sucrose TE buffer (10 mM Tris, 1mM EDTA), incubated with 100 mg/mL lysozyme for 37˚C
714 for 1 hr. After the cultures tarted to lyse, proteinase K, RNAse A, EDTA, Sarkosyl, and NaCl
715 was added. Phenol:Chloroform:IAA (25:24:1) was added to extract proteins, gently mixed, and
716 then the sample was pelleted to separate the phenol and aqueous layer. The aqueous layer was
717 then added to Chloroform:IAA (24:1), mixed gently, then centrifuged. The aqueous layer was
718 then precipitated using isopropanol and incubated at -20˚C for a minimum of 15 min. The
719 precipitated DNA was pelleted and then washed with 70% ethanol. The pellet was air dried and
720 then gently resuspended in 10 mM Tris pH 8.0 elution buffer.
721
722 *Genomic analyses.*
723 Genomic DNA was sequenced by MiGS at the University of Pittsburgh (now SeqCenter)
724 according to their standard protocol. Libraries were sequenced on an Illumina NextSeq 500
725 platform to generate paired-end 150 bp reads. Illumina reads of RT078 genomes were assembled
726 into contigs using SPAdes (v3.13.0),(76) and genes were called and annotated using Prokka
727 (v1.11) (77). Assembled and annotated contigs of five RT078 strains (TAL28131, TAL29600,
728 TAL29996, TAL30550, TAL30574) were applied for pangenomic analysis. Default settings
729 were used based on the Anvi'o workflow for microbial pangenomcis with adjustments for minbit
730 as 0.5 and mcl-inflation as 10(78-80). For SNPs analyses, reads of five RT078 genomes were
731 aligned to the reference M120 and variants were called by breseq (v. 0.38.1) by default
732 settings.(81)
733
734 *qPCR analyses*.
735 Each genomic DNA sample was analyzed by qPCR with primers that amplify the *cmr*-ON
736 sequence orientation, the *cmr*-OFF orientation, or the reference gene *rpoA* (32) . Each 20-µL
737 qPCR reaction consisted of 100 ng genomic DNA, 100 nM primers, and SensiMix™ SYBR®
738 reagents (Bioline). The reactions were run on a LightCycler® 96 (Roche Diagnostics), and *cmr*
739 switch orientation frequencies were calculated as described previously (44).
740
741 *Surface motility assays*

742 Starter cultures were grown until early stationary phase in BHIS then back-diluted 1:50 into
743 BHIS and grown until an OD_{600} of 0.5 was reached. 10 µL of the exponential-phase cultures
744 were then spotted onto BHIS plates and incubated at 37˚C for 5 days after which the plates were
745 scanned using a flatbed scanner.
746
747 *Mouse infection experiments*
748 Conventional 7-week-old C57BL/6 female mice from Jackson Laboratories were housed in a
749 sterile (autoclaved cage and bedding) large cage (24"x17") with autoclaved water and irradiated
750 food (Teklad 2918) for 10 days to allow for normalization of microbiota across mice through
751 coprophagy. After the 10-day normalization period, mice were started on cefoperazone, which
752 was added to their water at a concentration of 0.5mg/ml. Mice were allowed to drink the
753 cefoperazone water ad libitum for 10 days, after which they were placed back on sterile water
754 without antibiotic. After a 2-day period of being on normal sterile water, mice were weighed and
755 given a single dose of clindamycin (10mg/kg) via intraperitoneal injection. Immediately after IP
756 injection, mice were moved to standard-size autoclaved mouse cages (4 mice per cage) with
757 sterile food and water. 24 hours following the clindamycin injection, mice were inoculated with
758 1 x 10^5 spores of *C. difficile* (in 1xPBS) via oral gavage using a metal, reusable needle. Mice
759 were weighed by being placed in a plastic Nalgene cup on top of a scale. Fecal pellets were
760 collected just prior to oral gavage to ensure no prior *C. difficile* colonization and to note a
761 baseline weight. Following inoculation, mice were weighed to monitor % weight change over
762 time on days 1-4, 7, and 14. Fecal pellets were collected in duplicate on the same days for *C.*
763 *difficile* CFU enumeration and qPCR for detection of *cmr* switch orientation. On day 14, a
764 terminal weight was taken, and a fecal pellet was collected, followed by sacrifice via CO_2
765 inhalation with cervical dislocation as secondary method of euthanasia. Two experimental
766 replicates were completed using 4 mice per group, resulting in a total of 8 mice per condition.
767
768 *C. difficile CFU enumeration from mouse fecal pellets*
769 *C. difficile* engraftment in mice was monitored over a 14-day period. Fecal pellets were collected
770 from mice on days 0-4, 7, and 14. Each pellet was weighed and then suspended in 1x PBS. 10 µL
771 of the suspension was then serially diluted 1:10 in 1x PBS in a 96 well plate, and 5 µL was
772 spotted onto TCCFA agar to select for *C. difficile*, such that the dilutions plated were 2 x 10^3 – 2
773 x 10^7. *C. difficile* colonies were counted 24 hours after plating to allow for sufficient growth. *C.*
774 *difficile* CFUs were normalized by gram of fecal material.
775
776 *Data accessibility statement*
777 The data set and data processing scripts are publicly available
778 at https://doi.org/10.5281/zenodo.13352469 (82).
779
780 *Author contribution statement*
781 J.W.R. conducted all live-cell microscopy experiments and analyzed the single-cell data.
782 C.N. generated data visualizations from the time-lapse microscopy data, developed the method
783 for identifying septa within chains that had not initiated cell separation, and calculated
784 elongation rates and cell lengths. A. Singh advised C.N. in these quantitative analyses. I.N. and
785 A.S. conducted sporulation analyses and liquid culture experiments. J.W.R., R.T., and A.S.
786 conceptualized all experiments with input from A.Singh. Q.D. and A.S. extracted genomic
787 DNA and visualized cells at different growth phases. Q.D. conducted all the genomic analyses

788 and genome comparisons. N.D. and I.N. conducted spore purification analyses and imaging. N.
789 B.A. and I.E.M. developed and optimized methods for constructing agarose pads that could
790 support anaerobic growth in an ambient atmosphere. M.J.D. provided input on the DeLTA
791 analysis pipeline. N.D. conducted the animal experiments. A.M. conducted the qPCRs to
792 determine *cmr* switch orientation in Clade 5 isolates. The manuscript was written by J.W.R and
793 A.S with input from all authors.
794
795
796 **Table 1. *Clostridioides difficile* clinical isolates used in this study**
797

Strain Name	Clade	Ribotype	ST group	Source	Reference
630	1	012	2	Zurich, 1982 (Sanger Institute)	(83)
R20291	2	027	1	London, 2006 (Sanger Institute)	(84)
M68	4	017	81	Dublin, 2006 (Sanger Institute)	(50)
M120	5	078	11	UK, 2007 (Sanger Institute)	(50)
TAL28131	5	078	11	Tufts Medical Center	This paper
TAL29600	5	078	11	Tufts Medical Center	This paper
TAL29996	5	078	11	Tufts Medical Center	This paper
TAL30550	5	078	11	Tufts Medical Center	This paper
TAL30574	5	078	11	Tufts Medical Center	This paper
V48	5	078	11	Brigham & Women's Hospital	This paper
139b	5	078	11	Memorial Sloan Kettering	(20)
WU66	5	078	11	Barnes-Jewish Hospital	(20)
BBL2	1	012	2	Memorial Sloan Kettering	(20)
WU38	1	012	2	Barnes-Jewish Hospital	(20)
190B	1	087	46	Memorial Sloan Kettering	(20)
Wup14	2	027	1	Barnes-Jewish Hospital	(20)
BBL4	2	027	1	Memorial Sloan Kettering	(20)
186A	2	027	1	Memorial Sloan Kettering	(20)

798
799 Memorial Sloan Kettering Cancer Center (MSK), Barnes-Jewish Hospital (BJH)
800
801
802 **Table 2: Cell size and growth rate statistics for the studied strains.**
803

Strain Name	Clade	Mean Growth rate	Mean Cell Length (um)	S.D. Cell Length	Mean Chain Length (um)	S.D. Chain Length
630	1	1.63±0.02	8.51±0.06	2.24±0.04	12.53±0.11	3.46±0.07
R20291	2	1.88±0.01	not measured	not measured	11.72±0.08	3.15±0.05
M68	4	1.64±0.01	not measured	not measured	13.69±0.08	4.33±0.06
M120	5	2.15±0.01	not measured	not measured	21.8±0.2	10.2±0.2
TAL28131	5	2.17±0.02	11.15±0.06	3.34±0.04	19.7±0.2	6.9±0.1
TAL29600	5	2.11±0.02	14.0±0.1	4.44±0.08	29.1±0.4	13.1±0.3
TAL29996	5	2.15±0.02	9.44±0.04	2.70±0.03	13.65±0.06	3.87±0.04
TAL30550	5	2.05±0.04	11.82±0.08	3.34±0.05	27.3±0.3	9.8±0.3

V48	5	2.10±0.02	10.80±0.08	3.75±0.06	19.4±0.2	8.5±0.2

S.D. stands for standard deviation. The ± interval represents the 95% confidence interval of the estimated metric.

References

1. Desai K, Gupta SB, Dubberke ER, Prabhu VS, Browne C, Mast TC. 2016. Epidemiological and economic burden of *Clostridium difficile* in the United States: estimates from a modeling approach. BMC Infect Dis 16:303.
2. Guh AY, Mu Y, Winston LG, Johnston H, Olson D, Farley MM, Wilson LE, Holzbauer SM, Phipps EC, Dumyati GK, Beldavs ZG, Kainer MA, Karlsson M, Gerding DN, McDonald LC, Emerging Infections Program *Clostridioides difficile* Infection Working G. 2020. Trends in U.S. Burden of *Clostridioides difficile* Infection and Outcomes. N Engl J Med 382:1320-1330.
3. Shen A. 2020. *Clostridioides difficile* Spore Formation and Germination: New Insights and Opportunities for Intervention. Annu Rev Microbiol 74:545-566.
4. Abt MC, McKenney PT, Pamer EG. 2016. *Clostridium difficile* colitis: pathogenesis and host defence. Nat Rev Microbiol doi:10.1038/nrmicro.2016.108.
5. Theriot CM, Young VB. 2015. Interactions Between the Gastrointestinal Microbiome and *Clostridium difficile*. Annu Rev Microbiol 69:445-61.
6. Kordus SL, Thomas AK, Lacy DB. 2022. *Clostridioides difficile* toxins: mechanisms of action and antitoxin therapeutics. Nat Rev Microbiol 20:285-298.
7. Maroo S, Lamont J. 2006. Recurrent *Clostridium difficile*. Gastroenterology 130:1311-1316.
8. Zanella Terrier MC, Simonet ML, Bichard P, Frossard JL. 2014. Recurrent *Clostridium difficile* infections: the importance of the intestinal microbiota. World J Gastroenterol 20:7416-23.
9. Knight DR, Elliott B, Chang BJ, Perkins TT, Riley TV. 2015. Diversity and Evolution in the Genome of *Clostridium difficile*. Clin Microbiol Rev 28:721-41.
10. Knight DR, Imwattana K, Kullin B, Guerrero-Araya E, Paredes-Sabja D, Didelot X, Dingle KE, Eyre DW, Rodriguez C, Riley TV. 2021. Major genetic discontinuity and novel toxigenic species in *Clostridioides difficile* taxonomy. eLife 10.
11. Norsigian CJ, Danhof HA, Brand CK, Midani FS, Broddrick JT, Savidge TC, Britton RA, Palsson BO, Spinler JK, Monk JM. 2022. Systems biology approach to functionally assess the *Clostridioides difficile* pangenome reveals genetic diversity with discriminatory power. Proc Natl Acad Sci U S A 119:e2119396119.
12. Knight DR, Kullin B, Androga GO, Barbut F, Eckert C, Johnson S, Spigaglia P, Tateda K, Tsai PJ, Riley TV. 2019. Evolutionary and Genomic Insights into *Clostridioides difficile* Sequence Type 11: a Diverse Zoonotic and Antimicrobial-Resistant Lineage of Global One Health Importance. mBio 10.
13. Seth-Smith HMB, Biggel M, Roloff T, Hinic V, Bodmer T, Risch M, Casanova C, Widmer A, Sommerstein R, Marschall J, Tschudin-Sutter S, Egli A. 2021. Transition From PCR-Ribotyping to Whole Genome Sequencing Based Typing of *Clostridioides difficile*. Front Cell Infect Microbiol 11:681518.

848 14. Dingle KE, Elliott B, Robinson E, Griffiths D, Eyre DW, Stoesser N, Vaughan A,
849 Golubchik T, Fawley WN, Wilcox MH, Peto TE, Walker AS, Riley TV, Crook DW,
850 Didelot X. 2014. Evolutionary history of the *Clostridium difficile* pathogenicity locus.
851 Genome Biol Evol 6:36-52.
852 15. Mengoli M, Barone M, Fabbrini M, D'Amico F, Brigidi P, Turroni S. 2022. Make It Less
853 difficile: Understanding Genetic Evolution and Global Spread of *Clostridioides difficile*.
854 Genes (Basel) 13.
855 16. Clements AC, Magalhaes RJ, Tatem AJ, Paterson DL, Riley TV. 2010. *Clostridium*
856 *difficile* PCR ribotype 027: assessing the risks of further worldwide spread. Lancet Infect
857 Dis 10:395-404.
858 17. Endres BT, Begum K, Sun H, Walk ST, Memariani A, Lancaster C, Gonzales-Luna AJ,
859 Dotson KM, Basseres E, Offiong C, Tupy S, Kuper K, Septimus E, Arafat R, Alam MJ,
860 Zhao Z, Hurdle JG, Savidge TC, Garey KW. 2019. Epidemic *Clostridioides difficile*
861 Ribotype 027 Lineages: Comparisons of Texas Versus Worldwide Strains. Open Forum
862 Infect Dis 6:ofz013.
863 18. McDonald LC, Killgore GE, Thompson A, Owens RC, Jr., Kazakova SV, Sambol SP,
864 Johnson S, Gerding DN. 2005. An epidemic, toxin gene-variant strain of *Clostridium*
865 *difficile*. N Engl J Med 353:2433-41.
866 19. Dong Q, Lin H, Allen MM, Garneau JR, Sia JK, Smith RC, Haro F, McMillen T, Pope
867 RL, Metcalfe C, Burgo V, Woodson C, Dylla N, Kohout C, Sundararajan A, Snitkin ES,
868 Young VB, Fortier LC, Kamboj M, Pamer EG. 2023. Virulence and genomic diversity
869 among clinical isolates of ST1 (BI/NAP1/027) *Clostridioides difficile*. Cell Rep
870 42:112861.
871 20. Lewis BB, Carter RA, Ling L, Leiner I, Taur Y, Kamboj M, Dubberke ER, Xavier J,
872 Pamer EG. 2017. Pathogenicity Locus, Core Genome, and Accessory Gene Contributions
873 to *Clostridium difficile* Virulence. mBio 8.
874 21. Merrigan M, Venugopal A, Mallozzi M, Roxas B, Viswanathan VK, Johnson S, Gerding
875 DN, Vedantam G. 2010. Human hypervirulent *Clostridium difficile* strains exhibit
876 increased sporulation as well as robust toxin production. J Bacteriol 192:4904-11.
877 22. Shaw HA, Preston MD, Vendrik KEW, Cairns MD, Browne HP, Stabler RA, Crobach
878 MJT, Corver J, Pituch H, Ingebretsen A, Pirmohamed M, Faulds-Pain A, Valiente E,
879 Lawley TD, Fairweather NF, Kuijper EJ, Wren BW. 2020. The recent emergence of a
880 highly related virulent *Clostridium difficile* clade with unique characteristics. Clin
881 Microbiol Infect 26:492-498.
882 23. Li C, Harmanus C, Zhu D, Meng X, Wang S, Duan J, Liu S, Fu C, Zhou P, Liu R, Wu A,
883 Kuijper EJ, Smits WK, Fu L, Sun X. 2018. Characterization of the virulence of a non-
884 RT027, non-RT078 and binary toxin-positive *Clostridium difficile* strain associated with
885 severe diarrhea. Emerg Microbes Infect 7:211.
886 24. Imwattana K, Rodriguez C, Riley TV, Knight DR. 2021. A species-wide genetic atlas of
887 antimicrobial resistance in *Clostridioides difficile*. Microb Genom 7.
888 25. Kumar N, Browne HP, Viciani E, Forster SC, Clare S, Harcourt K, Stares MD, Dougan
889 G, Fairley DJ, Roberts P, Pirmohamed M, Clokie MRJ, Jensen MBF, Hargreaves KR, Ip
890 M, Wieler LH, Seyboldt C, Noren T, Riley TV, Kuijper EJ, Wren BW, Lawley TD. 2019.
891 Adaptation of host transmission cycle during *Clostridium difficile* speciation. Nat Genet
892 51:1315-1320.

893 26. Jain C, Rodriguez RL, Phillippy AM, Konstantinidis KT, Aluru S. 2018. High throughput
894 ANI analysis of 90K prokaryotic genomes reveals clear species boundaries. Nat Commun
895 9:5114.
896 27. Knetsch CW, Kumar N, Forster SC, Connor TR, Browne HP, Harmanus C, Sanders IM,
897 Harris SR, Turner L, Morris T, Perry M, Miyajima F, Roberts P, Pirmohamed M, Songer
898 JG, Weese JS, Indra A, Corver J, Rupnik M, Wren BW, Riley TV, Kuijper EJ, Lawley
899 TD. 2018. Zoonotic Transfer of *Clostridium difficile* Harboring Antimicrobial Resistance
900 between Farm Animals and Humans. J Clin Microbiol 56.
901 28. Hensgens MP, Keessen EC, Squire MM, Riley TV, Koene MG, de Boer E, Lipman LJ,
902 Kuijper EJ, European Society of Clinical M, Infectious Diseases Study Group for
903 Clostridium d. 2012. *Clostridium difficile* infection in the community: a zoonotic disease?
904 Clin Microbiol Infect 18:635-45.
905 29. Goorhuis A, Bakker D, Corver J, Debast SB, Harmanus C, Notermans DW, Bergwerff
906 AA, Dekker FW, Kuijper EJ. 2008. Emergence of *Clostridium difficile* infection due to a
907 new hypervirulent strain, polymerase chain reaction ribotype 078. Clin Infect Dis
908 47:1162-70.
909 30. Lim SC, Knight DR, Riley TV. 2020. *Clostridium difficile* and One Health. Clin
910 Microbiol Infect 26:857-863.
911 31. Bolton D, Marcos P. 2023. The Environment, Farm Animals and Foods as Sources of
912 *Clostridioides difficile* Infection in Humans. Foods 12.
913 32. Garrett EM, Sekulovic O, Wetzel D, Jones JB, Edwards AN, Vargas-Cuebas G, McBride
914 SM, Tamayo R. 2019. Phase variation of a signal transduction system controls
915 *Clostridioides difficile* colony morphology, motility, and virulence. PLoS Biol
916 17:e3000379.
917 33. Thanissery R, Winston JA, Theriot CM. 2017. Inhibition of spore germination, growth,
918 and toxin activity of clinically relevant C. difficile strains by gut microbiota derived
919 secondary bile acids. Anaerobe 45:86-100.
920 34. Ackermann M. 2015. A functional perspective on phenotypic heterogeneity in
921 microorganisms. Nat Rev Microbiol 13:497-508.
922 35. Aldridge BB, Fernandez-Suarez M, Heller D, Ambravaneswaran V, Irimia D, Toner M,
923 Fortune SM. 2012. Asymmetry and aging of mycobacterial cells lead to variable growth
924 and antibiotic susceptibility. Science 335:100-4.
925 36. Anjuwon-Foster BR, Tamayo R. 2017. A genetic switch controls the production of
926 flagella and toxins in *Clostridium difficile*. PLoS Genet 13:e1006701.
927 37. Anjuwon-Foster BR, Tamayo R. 2018. Phase variation of *Clostridium difficile* virulence
928 factors. Gut Microbes 9:76-83.
929 38. Kint N, Janoir C, Monot M, Hoys S, Soutourina O, Dupuy B, Martin-Verstraete I. 2017.
930 The alternative sigma factor sigma(B) plays a crucial role in adaptive strategies of
931 *Clostridium difficile* during gut infection. Environ Microbiol 19:1933-1958.
932 39. Courson DS, Pokhrel A, Scott C, Madrill M, Rinehold AJ, Tamayo R, Cheney RE,
933 Purcell EB. 2019. Single cell analysis of nutrient regulation of Clostridioides
934 (Clostridium) difficile motility. Anaerobe 59:205-211.
935 40. de Jong IG, Beilharz K, Kuipers OP, Veening JW. 2011. Live Cell Imaging of Bacillus
936 subtilis and Streptococcus pneumoniae using Automated Time-lapse Microscopy. J Vis
937 Exp doi:10.3791/3145.

938 41. Lugagne JB, Lin H, Dunlop MJ. 2020. DeLTA: Automated cell segmentation, tracking,
939 and lineage reconstruction using deep learning. PLoS Comput Biol 16:e1007673.
940 42. O'Connor OM, Alnahhas RN, Lugagne JB, Dunlop MJ. 2022. DeLTA 2.0: A deep
941 learning pipeline for quantifying single-cell spatial and temporal dynamics. PLoS
942 Comput Biol 18:e1009797.
943 43. Pogliano J, Osborne N, Sharp MD, Abanes-De Mello A, Perez A, Sun YL, Pogliano K.
944 1999. A vital stain for studying membrane dynamics in bacteria: a novel mechanism
945 controlling septation during Bacillus subtilis sporulation. Mol Microbiol 31:1149-59.
946 44. Garrett EM, Mehra A, Sekulovic O, Tamayo R. 2021. Multiple Regulatory Mechanisms
947 Control the Production of CmrRST, an Atypical Signal Transduction System in
948 *Clostridioides difficile*. mBio 13:e0296921.
949 45. Sauls JT, Cox SE, Do Q, Castillo V, Ghulam-Jelani Z, Jun S. 2019. Control of Bacillus
950 subtilis Replication Initiation during Physiological Transitions and Perturbations. mBio
951 10.
952 46. Eswaramoorthy P, Duan D, Dinh J, Dravis A, Devi SN, Fujita M. 2010. The threshold
953 level of the sensor histidine kinase KinA governs entry into sporulation in Bacillus
954 subtilis. J Bacteriol 192:3870-82.
955 47. Narula J, Kuchina A, Zhang F, Fujita M, Suel GM, Igoshin OA. 2016. Slowdown of
956 growth controls cellular differentiation. Mol Syst Biol 12:871.
957 48. Mehdizadeh Gohari I, Edwards AN, McBride SM, McClane BA. 2024. The impact of
958 orphan histidine kinases and phosphotransfer proteins on the regulation of clostridial
959 sporulation initiation. mBio 15:e0224823.
960 49. Deatherage DE, Traverse CC, Wolf LN, Barrick JE. 2014. Detecting rare structural
961 variation in evolving microbial populations from new sequence junctions using breseq.
962 Front Genet 5:468.
963 50. He M, Sebaihia M, Lawley T, Stabler R, Dawson L, Martin M, Holt K, Seth-Smith H,
964 Quail M, Rance R, Brooks K, Churcher C, Harris D, Bentley S, Burrows C, Clark L,
965 Corton C, Murray V, Rose G, Thurston S, van Tonder A, Walker D, Wren B, Dougan G,
966 Parkhill J. 2010. Evolutionary dynamics of *Clostridium difficile* over short and long time
967 scales. Proceedings of the National Academy of Sciences of the United States of America
968 107:7527-7532.
969 51. Sekulovic O, Mathias Garrett E, Bourgeois J, Tamayo R, Shen A, Camilli A. 2018.
970 Genome-wide detection of conservative site-specific recombination in bacteria. PLoS
971 Genet 14:e1007332.
972 52. Glomski IJ, Piris-Gimenez A, Huerre M, Mock M, Goossens PL. 2007. Primary
973 involvement of pharynx and peyer's patch in inhalational and intestinal anthrax. PLoS
974 Pathog 3:e76.
975 53. McKenney PT, Yan J, Vaubourgeix J, Becattini S, Lampen N, Motzer A, Larson PJ,
976 Dannaoui D, Fujisawa S, Xavier JB, Pamer EG. 2019. Intestinal Bile Acids Induce a
977 Morphotype Switch in Vancomycin-Resistant Enterococcus that Facilitates Intestinal
978 Colonization. Cell Host Microbe 25:695-705 e5.
979 54. Leslie JL, Jenior ML, Vendrov KC, Standke AK, Barron MR, O'Brien TJ, Unverdorben
980 L, Thaprawat P, Bergin IL, Schloss PD, Young VB. 2021. Protection from Lethal
981 *Clostridioides difficile* Infection via Intraspecies Competition for Cogerminant. mBio 12.

982 55. Theriot CM, Koumpouras CC, Carlson PE, Bergin, II, Aronoff DM, Young VB. 2011.
983 Cefoperazone-treated mice as an experimental platform to assess differential virulence of
984 *Clostridium difficile* strains. Gut Microbes 2:326-34.
985 56. Sachsenheimer FE, Yang I, Zimmermann O, Wrede C, Muller LV, Gunka K, Gross U,
986 Suerbaum S. 2018. Genomic and phenotypic diversity of *Clostridium difficile* during
987 long-term sequential recurrences of infection. Int J Med Microbiol 308:364-377.
988 57. Semenyuk EG, Poroyko VA, Johnston PF, Jones SE, Knight KL, Gerding DN, Driks A.
989 2015. Analysis of Bacterial Communities during *Clostridium difficile* Infection in the
990 Mouse. Infect Immun 83:4383-91.
991 58. Smith AB, Jenior ML, Keenan O, Hart JL, Specker J, Abbas A, Rangel PC, Di C, Green
992 J, Bustin KA, Gaddy JA, Nicholson MR, Laut C, Kelly BJ, Matthews ML, Evans DR,
993 Van Tyne D, Furth EE, Papin JA, Bushman FD, Erlichman J, Baldassano RN, Silverman
994 MA, Dunny GM, Prentice BM, Skaar EP, Zackular JP. 2022. Enterococci enhance
995 *Clostridioides difficile* pathogenesis. Nature 611:780-786.
996 59. Kim HY, Cho A, Kim JW, Kim H, Kim B. 2018. High prevalence of *Clostridium difficile*
997 PCR ribotype 078 in pigs in Korea. Anaerobe 51:42-46.
998 60. Moono P, Foster NF, Hampson DJ, Knight DR, Bloomfield LE, Riley TV. 2016.
999 *Clostridium difficile* Infection in Production Animals and Avian Species: A Review.
1000 Foodborne Pathog Dis 13:647-655.
1001 61. Burt SA, Siemeling L, Kuijper EJ, Lipman LJ. 2012. Vermin on pig farms are vectors for
1002 *Clostridium difficile* PCR ribotypes 078 and 045. Vet Microbiol 160:256-8.
1003 62. Dhungel BA, Govind R. 2021. Phase-variable expression of pdcB, a phosphodiesterase,
1004 influences sporulation in *Clostridioides difficile*. Mol Microbiol 116:1347-1360.
1005 63. Edwards AN, Willams CL, Pareek N, McBride SM, Tamayo R. 2021. c-di-GMP Inhibits
1006 Early Sporulation in *Clostridioides difficile*. mSphere 6:e0091921.
1007 64. Du S, Henke W, Pichoff S, Lutkenhaus J. 2019. How FtsEX localizes to the Z ring and
1008 interacts with FtsA to regulate cell division. Mol Microbiol 112:881-895.
1009 65. Li J, Xu X, Shi J, Hermoso JA, Sham LT, Luo M. 2023. Regulation of the cell division
1010 hydrolase RipC by the FtsEX system in Mycobacterium tuberculosis. Nat Commun
1011 14:7999.
1012 66. Pichoff S, Du S, Lutkenhaus J. 2019. Roles of FtsEX in cell division. Res Microbiol
1013 170:374-380.
1014 67. Xu X, Li J, Chua WZ, Pages MA, Shi J, Hermoso JA, Bernhardt T, Sham LT, Luo M.
1015 2023. Mechanistic insights into the regulation of cell wall hydrolysis by FtsEX and EnvC
1016 at the bacterial division site. Proc Natl Acad Sci U S A 120:e2301897120.
1017 68. Garcia-Garcia T, Poncet S, Cuenot E, Douche T, Giai Gianetto Q, Peltier J, Courtin P,
1018 Chapot-Chartier MP, Matondo M, Dupuy B, Candela T, Martin-Verstraete I. 2021.
1019 Ser/Thr Kinase-Dependent Phosphorylation of the Peptidoglycan Hydrolase CwlA
1020 Controls Its Export and Modulates Cell Division in *Clostridioides difficile*. mBio 12.
1021 69. Ransom EM, Williams KB, Weiss DS, Ellermeier CD. 2014. Identification and
1022 characterization of a gene cluster required for proper rod shape, cell division, and
1023 pathogenesis in *Clostridium difficile*. J Bacteriol 196:2290-300.
1024 70. Streett H, Charubin K, Papoutsakis ET. 2021. Anaerobic fluorescent reporters for cell
1025 identification, microbial cell biology and high-throughput screening of microbiota and
1026 genomic libraries. Curr Opin Biotechnol 71:151-163.

1027 71. Anjou C, Lotoux A, Zhukova A, Royer M, Caulat LC, Capuzzo E, Morvan C, Martin-
1028 Verstraete I. 2024. The multiplicity of thioredoxin systems meets the specific lifestyles of
1029 Clostridia. PLoS Pathog 20:e1012001.
1030 72. Shen A, Fimlaid KA, Pishdadian K. 2016. Inducing and Quantifying *Clostridium difficile*
1031 Spore Formation. Methods Mol Biol 1476:129-42.
1032 73. Ransom EM, Weiss DS, Ellermeier CD. 2016. Use of mCherryOpt Fluorescent Protein in
1033 *Clostridium difficile*. Methods Mol Biol 1476:53-67.
1034 74. Pishdadian K, Fimlaid KA, Shen A. 2015. SpoIIID-mediated regulation of sigma(K)
1035 function during *Clostridium difficile* sporulation. Mol Microbiol 95:189-208.
1036 75. Fimlaid KA, Jensen O, Donnelly ML, Francis MB, Sorg JA, Shen A. 2015. Identification
1037 of a Novel Lipoprotein Regulator of *Clostridium difficile* Spore Germination. PLoS
1038 Pathogens doi:10.1371/journal.ppat.1005239.
1039 76. Prjibelski A, Antipov D, Meleshko D, Lapidus A, Korobeynikov A. 2020. Using SPAdes
1040 De Novo Assembler. Curr Protoc Bioinformatics 70:e102.
1041 77. Seemann T. 2014. Prokka: rapid prokaryotic genome annotation. Bioinformatics
1042 30:2068-9.
1043 78. Benedict MN, Henriksen JR, Metcalf WW, Whitaker RJ, Price ND. 2014. ITEP: an
1044 integrated toolkit for exploration of microbial pan-genomes. BMC Genomics 15:8.
1045 79. Eren AM, Kiefl E, Shaiber A, Veseli I, Miller SE, Schechter MS, Fink I, Pan JN, Yousef
1046 M, Fogarty EC, Trigodet F, Watson AR, Esen OC, Moore RM, Clayssen Q, Lee MD,
1047 Kivenson V, Graham ED, Merrill BD, Karkman A, Blankenberg D, Eppley JM, Sjodin
1048 A, Scott JJ, Vazquez-Campos X, McKay LJ, McDaniel EA, Stevens SLR, Anderson RE,
1049 Fuessel J, Fernandez-Guerra A, Maignien L, Delmont TO, Willis AD. 2021. Community-
1050 led, integrated, reproducible multi-omics with anvi'o. Nat Microbiol 6:3-6.
1051 80. van Dongen S, Abreu-Goodger C. 2012. Using MCL to extract clusters from networks.
1052 Methods Mol Biol 804:281-95.
1053 81. Deatherage DE, Barrick JE. 2014. Identification of mutations in laboratory-evolved
1054 microbes from next-generation sequencing data using breseq. Methods Mol Biol
1055 1151:165-88.
1056 82. César N. 2024. Dataset for the article: Unique growth and morphology properties of
1057 Clade 5 *Clostridioides difficile* strains revealed by single-cell time-lapse microscopy. .
1058 Zenodo doi:https://doi.org/10.5281/zenodo.13352469.
1059 83. Sebaihia M, Wren B, Mullany P, Fairweather N, Minton N, Stabler R, Thomson N,
1060 Roberts A, Cerdeño-Târraga A, Wang H, Holden M, Wright A, Churcher C, Quail M,
1061 Baker S, Bason N, Brooks K, Chillingworth T, Cronin A, Davis P, Dowd L, Fraser A,
1062 Feltwell T, Hance Z, Holroyd S, Jagels K, Moule S, Mungall K, Price C, Rabbinowitsch
1063 E, Sharp S, Simmonds M, Stevens K, Unwin L, Whithead S, Dupuy B, Dougan G,
1064 Barrell B, Parkhill J. 2006. The multidrug-resistant human pathogen *Clostridium difficile*
1065 has a highly mobile, mosaic genome. Nature genetics 38:779-786.
1066 84. Stabler R, He M, Dawson L, Martin M, Valiente E, Corton C, Lawley T, Sebaihia M,
1067 Quail M, Rose G, Gerding D, Gibert M, Popoff M, Parkhill J, Dougan G, Wren B. 2009.
1068 Comparative genome and phenotypic analysis of *Clostridium difficile* 027 strains
1069 provides insight into the evolution of a hypervirulent bacterium. Genome biology 10.
1070